

Complex Analog Filters

W. Martin Snelgrove*, Adel S. Sedra*,
Gordon R. Lang**, and Peter O. Brackett**

ABSTRACT

This paper is concerned with the design of linear analog filters having transfer functions with complex-valued coefficients. Because their magnitude response is not symmetric around zero frequency, such filters have many interesting applications. These include the generation of single sideband signals and the sampling of bandpass signals. The paper presents approximation and realization methods for this class of filters.

-
- * W.M. Snelgrove and A.S. Sedra are with the Department of Electrical Engineering, University of Toronto, Toronto, Ontario, Canada M5S 1A4.
 - ** G.R. Lang and P.O. Brackett are with Motorola Information Systems, 9445 Airport Road, Brampton, Ontario L6S 4JL.
 - *** The research reported here was partially supported by the Defence Research Establishment, Atlantic, of the Canadian Department of National Defence.

Complex Analog Filters

W. Martin Snelgrove, Adel S. Sedra,
Gordon R. Lang and Peter O. Brackett

1. Introduction

This paper is concerned with the design of linear analog filters whose transfer functions $T(s)$ have complex-valued coefficients. Such a filter, referred to henceforth as a *complex analog filter*, has the advantage that its magnitude response, $|T(j\omega)|$, is not restricted to be symmetric around zero frequency. Thus, unlike "real" filters (that is, filters with transfer functions $T(s)$ having real-valued coefficients) whose attenuation requirements are posed on the semi-infinite frequency interval $0 \leq \omega \leq \infty$, a complex filter can be designed to meet attenuation requirements specified over the infinite frequency axis, $-\infty \leq \omega \leq \infty$, without regard to symmetry. This property permits novel and useful applications for complex filters.

The concept of complex filtering has been discussed in the technical literature for many years [1]-[11]. However, such treatments are usually in a theoretical setting wherein the introduction of complex signals is an artifice used to facilitate an analytic development. Indeed a wealth of theoretical material exists on the subject. Furthermore, a great deal has been reported on complex digital filters [12]-[14]. The corresponding literature in the analog case has been relatively sparse [15]-[20]. It is our objective here to show that complex analog filters may be considered as physical devices that can be

designed using simple and direct methods. In many cases these design techniques are extensions of those employed in the case of real filters.

Because complex filters are relatively unfamiliar to analog filter designers we present in Section 2 a tutorial exposition of the basic concepts involved. This section serves also to introduce some of the tools used in the design of complex filters.

In an attempt to motivate the study of complex filters two of their applications are described in Section 3. These are: the generation of single sideband (SSB) signals and the sampling of bandpass signals. The remainder of the paper is concerned with the design of complex filters: Approximation methods are given in Section 4 and realization techniques are presented in Section 5. The latter section includes also some experimental results.

2. Preliminaries

A complex filter $T(s)$ operates on a complex input signal $X(s)$ to produce a complex output signal $Y(s)$ according to

$$Y(s) = T(s)X(s)$$

Each of the functions $X(s)$, $Y(s)$ and $T(s)$ may in general have complex-valued coefficients. We shall begin with a brief discussion of complex analog signals.

2.1 Complex Analog Signals

One conventionally thinks of analog signals as being real-valued because

they are represented by (real-valued) voltages on wires. If, however, we have a pair of wires at different voltages (to ground, presumably) v_1 and v_2 we may think of the pair of wires as carrying the "complex voltage" $\Delta v = v_1 + jv_2$. Now, if v_1 and v_2 vary with time (that is, are signals) so does the fictitious signal v , and we call it a *complex analog signal*. This procedure is no different from that we follow when we write a complex number as, for instance, $3+j4$ or $(3,4)$: we are resolving the complex quantity (in a particular one of infinitely many possible ways) into an ordered pair of real numbers.

In the time domain a complex signal $x(t)$ is simply an ordered pair of real signals. We shall adopt the notation

$$x(t) \stackrel{\Delta}{=} x_R(t) + jx_I(t) \quad (1)$$

where the pair of real signals are assigned the subscripts R for real part and I for imaginary part of the complex signal.

By taking the Laplace transform of (1) we obtain

$$X(s) = X_R(s) + jX_I(s) \quad (2)$$

where $X_R(s)$ and $X_I(s)$, the Laplace transforms of $x_R(t)$ and $x_I(t)$ respectively, are functions with real-valued coefficients but $X(s)$ is (obviously) not. Evaluated for physical frequencies, $s = j\omega$, we find that

$$|X_R(-j\omega)| = |X_R(j\omega)|$$

$$\varphi[X_R(-j\omega)] = -\varphi[X_R(j\omega)]$$

$$|X_I(-j\omega)| = |X_I(j\omega)|$$

$$\varphi[X_I(-j\omega)] = -\varphi[X_I(j\omega)]$$

No such symmetries however exist for $|X(j\omega)|$.

To take a concrete and important example, if $x_R(t) = A \cos \omega_0 t$ and $x_I(t) = A \sin \omega_0 t$ where ω_0 is positive, then the complex signal $x(t)$ is given by

$$x(t) = A(\cos \omega_0 t + j \sin \omega_0 t) = Ae^{j\omega_0 t}$$

which has power only at the positive frequency ω_0 . On the other hand the real signal $x_R(t)$ is given by

$$x_R(t) = A \cos \omega_0 t = \frac{1}{2} A(e^{j\omega_0 t} + e^{-j\omega_0 t})$$

and thus must have power at the frequencies ω_0 and $-\omega_0$.

2.2 Complex Transfer Functions

Consider next the complex transfer function $T(s)$. Such a transfer function can always be written uniquely as

$$T(s) = T_R(s) + jT_I(s) \quad (3)$$

where $T_R(s)$ and $T_I(s)$ are functions with real-valued coefficients.

Example (1)

Consider a first-order complex low-pass filter having the transfer function

$$T(s) = \frac{1}{s + 1 - j} \quad (4)$$

This filter has a single complex pole (natural mode) at $-1+j$ and has the magnitude and phase responses shown in Fig. 1. It may be observed that the

transfer function in (4) can be obtained from that of the first-order real low-pass filter [$1/(s+1)$] by replacing s by $(s-j)$. This is confirmed by the plots in Fig. 1 which are those of the real filter [$1/(s+1)$] shifted up the ω axis by $\Delta\omega=1$. Another interesting observation to make from the plots in Fig. 1 is that the complex filter can be viewed as a bandpass filter whose magnitude response is maximally-flat around the center-frequency $\omega=1$. This bandpass filter has the further interesting property that its magnitude response is arithmetically symmetric around the center-frequency.

Multiplying the numerator and denominator of the complex transfer function in (4) by the complex conjugate of the denominator results in

$$T(s) = \frac{s+1}{s^2+2s+2} + j \frac{1}{s^2+2s+2} \quad (5)$$

Thus,

$$T_R(s) = \frac{s+1}{s^2+2s+2} \quad (6)$$

and

$$T_I(s) = \frac{1}{s^2+2s+2} \quad (7)$$

Note that $T_R(s)$ and $T_I(s)$ have real coefficients and thus can be realized in the usual fashion. At this point it is also useful to observe that $T_R(s)$ and $T_I(s)$ have the same poles. This enables the realization of $T_R(s)$ and $T_I(s)$ within the same network, as will be shown later.

2.3 Representation of Complex Filters

Consider the application of a complex signal $X(s)$ to the input of a complex filter $T(s)$. At the output we obtain the complex signal $Y(s)$ given by

$$\begin{aligned} Y(s) &= T(s)X(s) \\ &= [T_R(s) + jT_I(s)][X_R(s) + jX_I(s)] \\ &= [T_R(s)X_R(s) - T_I(s)X_I(s)] + j[T_I(s)X_R(s) + T_R(s)X_I(s)] \end{aligned}$$

Thus the complex output signal $Y(s)$ has the two real components $Y_R(s)$ and $Y_I(s)$ given by

$$Y_R(s) = T_R(s)X_R(s) - T_I(s)X_I(s) \quad (8)$$

$$Y_I(s) = T_I(s)X_R(s) + T_R(s)X_I(s) \quad (9)$$

Equations (8) and (9) lead to a number of ways for representing complex filters, as illustrated in Fig. 2. Fig. 2a provides a black-box representation of the system, where, to emphasize the complex nature of the input and output signals, double lines are used. In Fig. 2b we show a complex signal-flow-graph (SFG) representation of the complex filter. Again we note the use of double lines.

Fig. 2c shows a block diagram realization of the complex filter $T(s)$ using four separate real circuits and two summers. This realization is a direct implementation of Eqns. (8) and (9). As noted earlier, however, the functions $T_R(s)$ and $T_I(s)$ have the same natural modes and can thus be realized within the same network. In other words, while the block diagram of Fig. 2c serves to illustrate the realizability of complex transfer functions using physical cir-

cuits, it is not necessary to realize a complex filter in this manner. Furthermore, although in general a complex transfer function is realized as a two-input two-output system, there are many applications where the input signal is real, and there are other applications in which one is interested in only one of the two components of the output signal. In such cases more economic realizations are possible.

Finally we show in Fig. 2d a "real" SFG representation of the realization in Fig. 2c. Note that this real SFG is equivalent to the complex SFG of Fig. 2b. This equivalence which is shown explicitly in Fig. 3 is frequently employed to convert a complex SFG realization of a complex transfer function into a real SFG, as illustrated in the following Example.

Example (2)

The 1st order complex filter of Example (1) whose transfer function is given in Eqn. (4) can be realized (to within a gain constant of -1) by the complex SFG shown in Fig. 4a. This SFG is obtained directly from the transfer function by recognizing that the transfer function is that of an inverting integrator ($-1/s$) with a feedback transmittance of $(1 - j)$. Using the identity of Fig. 3 the complex SFG of Fig. 4a can be converted to the real SFG of Fig. 4b.

Using op-amp circuits, one can obtain a circuit implementation of the complex first-order filter directly from the SFG of Fig. 4b. Such a circuit is shown in Fig. 4c. As expected, the realization is a two-input two-output circuit. If however, the input signal is real than the "imaginary" input terminal and its associated feed-in resistor can be eliminated. It is useful to observe that the circuit in Fig. 4c is basically a two-integrator loop that realizes the second

order denominator polynomial of Eqns. (5)-(7). Note that $T_R(s)$ and $T_I(s)$ are indeed realized within the same network. From Eqns. (8) and (9) we see that $T_R(s)$ can be measured as $Y_R(s)/X_R(s)$ with $X_I(s)=0$ or equivalently as $Y_I(s)/X_I(s)$ with $X_R(s)=0$. Similarly $T_I(s)$ is $Y_I(s)/X_R(s)$ with $X_I(s)=0$ or $-Y_R(s)/X_I(s)$ with $X_R(s)=0$. These results apply for any general complex filter.

3. Applications

In this section we describe two applications of complex filters: a direct method for the generation of single-sideband (SSB) signals, and a method for the sampling of bandpass signals.

3.1 Generation of SSB Signals

The well-known phase-shift method for generating SSB signals [21] consists of shifting the phase of the baseband signal by 90° and then feeding the signal together with its phase-shifted version to a quadrature modulator. In this scheme the phase shifter is required to provide a constant 90° phase shift over the entire bandwidth of the baseband signal. Errors in the phase or gain response of the shifter translate into reduced attenuation of the suppressed sideband. The problem of designing such a wideband phase shifter is a challenging one.

To simplify the design of the phase-shift SSB modulator a variation on the scheme described above is usually employed [18]. The block diagram of such a modulator is shown in Fig. 5. The input signal is first fed to a low-pass filter

which limits the bandwidth of the baseband signal to the allotted channel width. The filtered baseband signal is then fed to a pair of all-pass networks which are designed to produce a pair of signals $x_1(t)$ and $x_2(t)$ that are 90° apart in phase. These two signals are then fed to the quadrature modulator, as shown.

In this scheme the problem of designing a 90° wideband phase shifter is replaced by that of designing a pair of all-pass networks whose outputs are 90° apart in phase. Although simpler, the design of this pair of all-pass networks is by no means trivial. Also, it is not easy to directly relate the specification and performance of the SSB modulator to the specification and performance of the pair of all-pass networks. Finally, once designed the lack of coupling between the two channels makes implementations very sensitive to mismatches.

Before presenting our proposed approach to the design of SSB modulators we wish to make an important observation on the system of Fig. 5. The pair of all-pass networks can be considered a complex filter with a single input and two outputs. Since the two outputs of this complex filter have 90° of phase difference the complex filter is in effect generating the analytic signal [6,10] corresponding to the input signal. It can be shown that this complex filter is ideally a *positive pass* filter; that is, a filter that passes all positive frequencies and stops all negative frequencies. The two output signals of an ideal positive-pass filter are interrelated by the Hilbert transform.

The above observation leads directly to the proposed method for SSB generation. Fig. 6a illustrates the technique. The input signal is fed to the real input terminal of a complex bandpass filter. As indicated, this filter serves the dual purpose of limiting the bandwidth of the baseband signal as well as

attenuating its negative-frequency components. The complex filter thus delivers at its output an SSB baseband signal. Multiplying this signal by the complex carrier wave $V_c e^{j\omega_c t}$ shifts the spectrum up the $j\omega$ -axis as indicated in the diagram. Then, simply taking the real part of the resulting complex signal provides the required SSB signal.

There are four advantages of the method of Fig. 6a over the well-known scheme of Fig. 5. First the specifications and performance of the system can be directly related to those of the filter: If, for instance, 40 dB of lower sideband suppression is required then the filter should be designed to provide 40 dB of attenuation over the negative frequency band. Similarly, if 0.5 dB of amplitude variation over the channel bandwidth is allowed then the filter passband should be specified to have a maximum ripple of 0.5 dB. Note that no mention is made of phase shift.

The second advantage of the method of Fig. 6a is the ease of designing the complex filter (as compared to designing wideband phase shifters). We shall provide in this paper systematic procedures for designing and implementing complex filters of this type.

Thirdly, the modulator proposed in Fig. 6a provides economy of implementation resulting from combining the filtering and the 90° phase-shifting functions (which are separately performed in the modulator of Fig. 5) into one block; the complex bandpass filter.

Finally, as will be shown in this paper, there exist design methods that result in complex-filter implementations with strong coupling between their two channels. Such implementations feature low sensitivities especially when compared to the usual implementations of the SSB modulator.

To further illustrate the proposed method we show in Fig. 6b a block diagram for its implementation. Note that because only the real part of the output is required only two multipliers are needed to implement the complex multiplication of Fig. 6a. Now compare the block diagrams of Figs. 5 and 6b. It is readily seen that the combination of low-pass filter followed by the pair of all-pass networks is nothing but a special case of the complex bandpass filter of Fig. 6b. It should be clear, however, that this special case is inefficient, awkward to specify and difficult to design.

3.2 Complex Sampling of Bandpass Signals

As another application of complex filters consider the process of sampling bandpass signals such as the one whose spectrum is shown in Fig. 7a. There are basically two approaches that enable sampling this signal at a rate of W rad/s; both involve complex sampling. The first approach [10,22] consists of demodulating the bandpass signal by multiplying it by the complex carrier $e^{-j\omega_c t}$. This simply shifts the spectrum to baseband, as indicated in Fig. 7b. Note that since the spectrum of the resulting signal is no longer symmetric around zero frequency, it is obvious that the demodulated signal is complex. To eliminate the part of spectrum centered around $-2\omega_c$, as well as to limit the band of the signal to $\pm W/2$, a real low-pass filter centered at zero frequency is used, as illustrated in Fig. 7b. Although this is a real filter, it operates on a complex signal and hence consists of two channels, as indicated in Fig. 8. The resulting complex baseband signal can now be sampled at a rate of W rad/s. Note that as indicated in Fig. 8 there are two channels to sample and we may consider the samples as complex.

An alternative approach that is simpler consists of passing the real bandpass signal of Fig. 7a through a complex bandpass filter centered at ω_c and with a bandwidth W . This will have the effect of eliminating the negative frequency components of the spectrum. Thus at the output of the complex bandpass filter we obtain the positive part of the bandpass signal, as indicated in Fig. 9. This latter signal is obviously complex. It can be sampled at the rate of W rad/s. As shown in Fig. 9, here too there are two channels to sample; in other words, the samples are complex. Although the sampling rate is the same as in the first scheme the need for demodulation has been obviated (it is implicit in the sampling). Finally, it should be mentioned that in applications where ω_c is low the usual practice is to sample at a rate of $2(\omega_c + \frac{W}{2})$. Therefore adopting the approach proposed here would result in some economy.

4. Approximation

In this section we address the problem of obtaining a complex transfer function $T(s)$ [or $H(s)$ where $H(s) = 1/T(s)$] whose associated attenuation function $A(\omega) \equiv 20\log|H(j\omega)|$ meets given specifications. Although an extensive theory is available [23,24] for the approximation of conjugate specifications by transfer functions with real coefficients, the corresponding theory for complex filters is limited: Lang and Brackett [19] suggest an approximation technique based on a narrow-band approximation, while Tsuchiya and Shida [18] develop a theory for a special case in which natural modes are pure real but transmission and reflection zeros complex. We give here the complex equivalent of the exact formulae available in real-filter design. These formulae should allow one to rewrite standard filter approximation routines to handle

the complex case. We also give a number of methods to transform between complex and real filters to allow designers to use existing computer programs to design complex filters.

4.1 An Approximation Method Based on the Narrow Band Approximation

We shall begin by describing the approximation method proposed in [19]. It involves shifting the attenuation specifications of the complex filter up the frequency axis by an amount much greater than the filter bandwidth. The shifted specifications would then appear as those of a narrow-band bandpass filter. This bandpass filter can be turned into a real filter by adding the conjugate negative-frequency specifications. The resulting specifications can then be approximated using a standard (real-filter) approximation routine.

The conjugate transfer-function singularities obtained from the approximation routine are then processed as follows: the lower-half-plane set is discarded and the upper-half-plane set is shifted down the frequency axis by an amount equal to the original upward shift of specifications. This translated set of singularities which do not necessarily have conjugate symmetry then form the desired set for the complex filter to be realized. Note that in discarding the lower-half-plane singularities we are relying on the validity of the narrow-band approximation; namely that the center frequency of the real filter is so great that the interaction between conjugate singularities is negligible.

Example (3)

Let it be required to design a complex bandpass filter with the following specifications:

Passband: $600\text{Hz} \leq f \leq 1100\text{Hz}$ with 1.0 dB equiripple

Lower Stopband: $-\infty \leq f \leq 0$ with a minimum of 35 dB attenuation

Upper Stopband: $3600\text{Hz} \leq f \leq \infty$ with a minimum of 30 dB attenuation

For input to a standard computer routine (in this case the filter design package APSYN [25] was used) a displacement of 999,400 Hz was added to all critical specification frequencies to achieve the narrow-band approximation. Doing this and adding mirror-image specifications on the negative frequency axis results in the specifications for a real bandpass filter having a passband from 1,000,000 Hz to 1,000,500 Hz, together with appropriate stopbands.

After allowing APSYN to find a solution to this problem, a fourth-order general parameter bandpass filter having the following set of singularities was obtained:

Natural modes: $-169.6623888 \pm j 1,000,455.978\text{Hz}$

$-107.2482974 \pm j 1,000,012.356\text{Hz}$

Transmission Zeros: $0.0 \pm j 999,250.4756\text{Hz}$

$\pm \infty$

The natural modes and transmission zeros of the complex filter were then obtained by simply subtracting 999,400 Hz from the positive-frequency imaginary parts of the real filter. The set of singularities for the complex filter were then to be

Natural Modes: $s_1 = -169.6623888 + j 1,055.978\text{Hz}$

$s_2 = -107.2482974 + j 612.3563\text{Hz}$

Transmission Zeros: $s_3 = 0.0 - j 149.52445 \text{Hz}$

$s_4 = \infty$

Fig. 10 shows the computed attenuation and phase characteristics of this complex filter.

Although this method is approximate it yields good results in many applications.

4.2 An Approximation Method for Arithmetically-Symmetric Complex Bandpass Filters

If the complex filter to be designed is bandpass with attenuation specifications that are arithmetically symmetric around the center frequency then a simple and exact method is available for obtaining a suitable transfer function. To illustrate this method consider Fig. 11a which shows typical specifications for an arithmetically-symmetric complex bandpass filter. The first step in the approximation process consists of linearly shifting the specifications so that the center frequency ω_0 coincides with the origin of a new axis, the Ω axis in Fig. 11b. Since the shifted specifications are symmetric around the origin of the Ω axis, standard (real-filter) approximation methods can be applied. For illustration let us assume that a third-order elliptic function meets the shifted specifications. A sketch of the corresponding attenuation function is shown in Fig. 11b.

Denoting the real transfer function in Fig. 11b $H(p)$ then the complex transfer function that meets the original specifications of Fig. 11a is $H(p)|_{p=s-j\omega_0}$. Fig. 11c shows the frequency response of the resulting third-

order complex bandpass filter. It will be shown in Section 5.4 that complex filters designed in this manner have interesting and simple realizations. Finally note that the first-order complex bandpass filter whose $|T(j\omega)|$ is shown in Fig. 1 is arithmetically symmetric and can be obtained by shifting the magnitude response of a first-order real low-pass filter.

4.3 Feldtkeller's Equation

We shall next address the question of adapting the approximation theory of real filters to the complex case. Towards that end we note that it is generally easier to approximate characteristic functions $K(s)$ (ideally 0 in passbands and ∞ in stopbands) than transfer functions $H(s)$ (ideally 1 in passbands and ∞ in stopbands). In real-filter design, Feldtkeller's equation allows one to derive an $H(s)$ from any $K(s)$ such that

$$|H(j\omega)|^2 = 1 + |K(j\omega)|^2 \quad (10)$$

[Note that the passband ripple factor ε has been absorbed in $K(s)$].

This much applies equally well to complex filters. In real filters a pair of identities is then used to produce an equation in rational functions that reduces to Eqn. (10) over the $j\omega$ axis. For any rational function $M(s)$ with real coefficients

$$|M(s)|_{s=j\omega}^2 = M(s)\overline{M(s)}|_{s=j\omega} \quad (11)$$

$$= M(s)M(-s)|_{s=j\omega} \quad (12)$$

where $\overline{M(s)}$ is the conjugate of $M(s)$, so that Eqn. (10) may be rewritten

$$H(s)H(-s)=1+K(s)K(-s) \quad (13)$$

Now this is *not* directly applicable to complex filters, because (12) only holds when $M(s)$ has real coefficients. Eqn. (11) still applies but cannot be used directly because $\bar{M}(s)$ is not a rational function of s , which is why (12) was needed to analytically continue (10) from the imaginary axis to the whole s -plane. To solve this problem we define a function $\bar{M}(s)$, so that $\bar{M}(s)$ has coefficients conjugate to those of $M(s)$. We then have

$$\bar{M}(s)=\bar{M}(\bar{s})$$

and on $s=j\omega$, $\bar{s}=-s$, so

$$|M(s)|^2_{s=j\omega}=M(s)\bar{M}(-s)|_{s=j\omega}$$

and now the right-hand-side is rational*. Our new version of (13), then, is

$$H(s)\bar{H}(-s)=1+K(s)\bar{K}(-s) \quad (14)$$

from which, by looking at the numerator and denominator polynomials,

$$H(s)=\frac{E(s)}{P(s)}$$

$$K(s)=\frac{F(s)}{P(s)}$$

we can derive a formula in polynomials

$$E(s)\bar{E}(-s)=F(s)\bar{F}(-s)+P(s)\bar{P}(-s) \quad (15)$$

This formula is suitable for computation of $E(s)\bar{E}(-s)$ from a given $K(s)$, and produces roots symmetrical about the $j\omega$ axis, so that pole sorting may be used to construct a stable $E(s)$.

* Kuh and Rohrer [8] use complex power definitions like this for their discussion of complex one-port networks.

Example (4)

Consider a first-order complex filter with a reflection zero at $s=j1$ and a loss pole at $s=-j1$, that is

$$F(s)=s-j$$

and,

$$P(s)=s+j$$

then

$$\begin{aligned}E(s)\bar{E}(-s) &= (s-j)(-s+j) + (s+j)(-s-j) \\&= 2(1-s)(1+s)\end{aligned}$$

and we can sort roots to obtain

$$E(s)=\sqrt{2}(s+1)$$

This filter which has a transfer function $T(s)$ given by

$$T(s)=\frac{P(s)}{E(s)}=\frac{1}{\sqrt{2}} \frac{s+j}{s+1}$$

provides a first-order approximation to an SSB filter specification. Note that the fact that $E(s)$ happened to have real coefficients is a coincidence arising from the symmetrical relationship between $F(s)$ and $P(s)$. This symmetrical case is the one studied by Tsuchiya and Shida [18], although much of their work can be applied more generally.

The availability of a form of Feldtkeller's equation for complex filters makes it possible to obtain transfer functions from given characteristic functions. Characteristic functions may be obtained by doing simultaneous approximation on passbands and stopbands after the fashion of [26]; by using classical

approximations (e.g. Chebyshev polynomials); or by using an approximator on stopband specifications together with closed-form expressions for $F(s)$ that result in the desired passband [23,24]. For the latter approach we give the complex-equivalent of the transformed-variable method [27,24] usually employed in real-filter design in Section 4.5. Before we do that, however, we shall describe another transformation that enables the approximation of complex specifications using a real filter prototype.

4.4 A Transformation Between Real and Complex

In this section we present a transformation between the frequency variable s of the complex filter to be designed and the frequency variable p of a corresponding real filter prototype. It will be shown that this transformation enables the approximation of complex specifications that are in general not symmetric but which are restricted to the positive $j\omega$ axis. This restriction can usually be overcome by shifting the specifications to the positive ω region. For the cases where this cannot be done (that is, where the filter is specified down to $\omega = -\infty$) we shall present an extension of the transformation.

The transformation is

$$s = p^2 / j \quad (16)$$

It changes a real-filter transfer function $H_r(p)$ of order N into a complex-filter transfer function $H(s)$ of order $N/2$. The transformation maps conjugate frequencies along the $j\Omega$ axis (the imaginary axis in the p plane), i.e. $p = \pm j\Omega$, to single frequencies along the positive $s = j\omega$ axis with

$$\omega = \Omega^2 \quad (17)$$

Real axis points in the p plane map to locations on the negative $s = j\omega$ axis. It follows that if this transformation is to yield a stable function $H(s)$ then the prototype function $H_r(p)$ must have no real natural modes. It should also be apparent that the order N of the prototype real filter must be even.

A direct application of (16) to a transfer function $H_r(p)$ would result in \sqrt{s} terms. This problem can be avoided by applying the transformation to the squared transfer function $H_r(p)H_r(-p)$. The result will be the squared function $H(s)\bar{H}(-s)$ and the complex filter will have the same magnitude response as that of the real prototype.

Finally, we note that the natural modes of the complex filter can be obtained from those of the real filter (e_i, \bar{e}_i) as e_i^2/j or \bar{e}_i^2/j ; the selection between the two should be done for stability.

Example (5)

Let it be required to design a complex filter (for an SSB application) to meet the attenuation specifications shown in Fig. 12a. We first shift the specifications to positive frequencies and normalize with the linear transformation

$$\tilde{s} = \frac{s + 2\pi \times 4000j}{2\pi \times 7300},$$

thus obtaining the new set of specifications depicted in Fig. 12b. Now to obtain the specifications of the real-filter prototype we must take account of the relationship in Eqn. (17). That is, we must prewarp the frequency axis using $\Omega = \sqrt{\tilde{\omega}}$, where Ω denotes frequency in the real-filter prototype domain and

$\tilde{\omega} = \text{Im}(\tilde{s})$. The specifications thus obtained for the real-filter prototype are shown in Fig. 12c. Also shown is the magnitude response of an eighth-order filter that satisfies the specifications and that was obtained using the standard filter approximation routine available in the FILTOR 2 package [28]. We can now apply the transformation $p^2 = \tilde{j}\tilde{s}$ to obtain the transfer function of the complex filter that meets the specifications of Fig. 12b. This can be simply done by transforming the roots e_i, p_i of the real filter using: $\tilde{e}_{ic} = e_i^2/j$ and $\tilde{p}_{ic} = p_i^2/j$. Finally the singularities e_{ic}, p_{ic} of the complex transfer function that satisfies the original specifications of Fig. 12a can be obtained by denormalizing \tilde{e}_{ic} and \tilde{p}_{ic} by 7300 Hz and shifting the resulting roots down the frequency axis by 4000 Hz, that is,

$$e_{ic} (\text{or } p_{ic}) = 2\pi \times 7300 \tilde{e}_{ic} (\text{or } \tilde{p}_{ic}) - 2\pi \times 4000 j$$

Fig. 12d shows a sketch of the original specifications together with the magnitude response of the fourth-order complex transfer function thus obtained. The loss poles, reflection zeros, and natural modes of this function are:

Polynomial	$P(s)$	$F(s)$	$E(s)$
Leading Coefficient	50.801	15988	5584.8
Roots (normalized to 7300 Hz)	-j0.20518	j0.04911	-0.017533 + j0.038052
	-j0.051846	j0.12327	-0.06854 + j0.10648
	j0.9011	j0.28484	-0.10938 + j0.28667
	∞	j0.43072	-0.049279 + j0.45674

Because the transformation $s = p^2/j$ only attends to positive frequencies it was required to first shift the given specifications so that all specified points were at positive frequencies. Unfortunately this cannot be done if the complex filter is specified down to $\omega = -\infty$. This limitation can be overcome by preceding the transformation $s = p^2/j$ by another transformation that maps the lower transition band in the complex filter specifications onto the entire negative frequency axis. To be specific, consider the design of a complex bandpass filter having the attenuation specifications shown in Fig. 13a. The mapping

$$\tilde{s} = j\alpha \frac{s - j\omega_{PL}}{s - j\omega_{SL}} \quad (18)$$

transforms the specifications to the set shown in Fig. 13b versus $\tilde{\omega} = \text{Im}(\tilde{s})$ where

$$\tilde{\omega}_P = \alpha \frac{\omega_{PH} - \omega_{PL}}{\omega_{PH} - \omega_{SL}}$$

$$\tilde{\omega}_S = \alpha \frac{\omega_{SH} - \omega_{PL}}{\omega_{SH} - \omega_{SL}}$$

Note that the lower transition band, $\omega_{SL} \leq \omega \leq \omega_{PL}$, is mapped onto $-\infty \leq \tilde{\omega} \leq 0$, while the rest of the specification bands are mapped onto the positive $\tilde{\omega}$ axis. Now the specifications in Fig. 13b are in the form suitable for applying the transformation $\tilde{s} = p^2/j$. Finally, we note that the constant α in Eqn. (18) may be used to normalize the specifications. For instance, by selecting

$$\alpha = \frac{\omega_{PH} - \omega_{SL}}{\omega_{PH} - \omega_{PL}} \quad (19)$$

the upper passband edge is normalized to $\tilde{\omega} = 1$.

Example (6)

Let it be required to design a complex filter with a passband from dc to +3000 Hz and with stopbands extending up from 4000 Hz and down from -1000 Hz. Passband ripple is to be 0.1 dB and we want 40 dB of stopband attenuation. In terms of the parameters of Fig. 13a we have

$$\omega_{SL} = -2\pi \times 1000 \text{ rad/s} \quad \omega_{PL} = 0 \quad \omega_{PH} = 2\pi \times 3000 \text{ rad/s}$$

$$\omega_{SH} = 2\pi \times 4000 \text{ rad/s} \quad A_P = 0.1 \text{ dB} \quad A_{SL} = A_{SH} = 40 \text{ dB}$$

Selecting α according to Eqn. (19),

$$\alpha = \frac{3000+1000}{3000-0} = \frac{4}{3}$$

results in the transformation of Eqn. (18) given by

$$\tilde{s} = j \frac{4}{3} \frac{s}{s + j2\pi \times 1000} \quad (20)$$

and the specifications become those in Fig. 13b with $\tilde{\omega}_P = 1$, $\tilde{\omega}_S = \frac{16}{15}$, $A_P = 0.1 \text{ dB}$, and $A_{SH} = A_{SL} = 40 \text{ dB}$. Now prewarping the frequency axis using $\Omega = \sqrt{\tilde{\omega}}$, and adding the conjugate specifications yields the specifications for the real filter prototype.

A transfer function that meets the real-filter specifications can be obtained from filter tables. Specifically, an elliptic function of order 9 would satisfy the specifications. However, to be able to use our transformation we must have an even-order prototype filter. Thus, selecting an elliptic function with $N=10$ and applying the transformations $p^2 = \tilde{s}$ and $\tilde{s} = j \frac{4}{3} \frac{s}{s + j2\pi \times 1000}$ we obtain a fifth-order complex filter satisfying the original specifications. Finally, note

that because the original specifications are arithmetically symmetric around $f_0 = 1500\text{Hz}$, the method of Section 4.1 could have equally well been used and in fact yields an identical result.

4.5 Direct Approximation Using Transformed Variables

Rather than transforming a real prototype, the approximation problem for complex filters can be solved directly using an adaptation of the transformed variable method [27] that is popular in the design of real filters. To develop this adaptation we recall that the transformed-variable method is based on the following mapping between the real-filter plane (referred to here as the p plane) and another complex-variable plane, the z plane,

$$z^2 = \frac{p^2 + 1}{p^2 + a^2} \quad (21)$$

where a and 1 are the edges of the filter passband along the $p = j\Omega$ axis.

Secondly, we recall that we are able to transform between real and complex using

$$s = p^2 / j \quad (22)$$

These two mappings may be collapsed into a single transformation between the complex-filter plane (s plane) and the transformed-variable plane (z plane), namely

$$z^2 = \frac{s - j\omega_{PH}}{s - j\omega_{PL}} \quad (23)$$

where ω_{PL} and ω_{PH} denote the edges of the passband of the complex filter along the $s = j\omega$ axis.

The z-plane closed-form expressions available for the design of real filters can be easily modified for the general complex case. For instance, to obtain an equiripple passband the formula relating the squared reflection zeros and the squared loss poles becomes

$$F(z)\bar{F}(-z) = [P_{ev}(z)]^2 \quad (24)$$

where the subscript ev denotes "even part". This formula can be used in an iterative approximation routine (pole placer) to optimally locate the loss poles (that is, to obtain an equiminima stopband attenuation) while automatically ensuring the equiripple nature of the passband. The modified Feldtkeller equation can then be used to determine the natural modes.

It is worth noting that the mapping in Eqn. (23) has a somewhat different effect than the corresponding mapping for real filters in Eqn. (21). Specifically, both transformations map the passband over the entire imaginary axis of the z-plane, and map the upper transition band and stopband onto the region of the real axis between -1 and 1. In the complex case, the transformation maps the lower transition band and stopband onto the portions of the real axis $|z| \geq 1$. Furthermore, note that the order of transfer function is halved in going from z to s .

Example (7)

Consider a first-order complex filter with a passband between $\omega_{PL}=0$ and $\omega_{PH}=1\text{rad/s}$ and with a single loss pole at $\omega=-1\text{rad/s}$. The z mapping in this case becomes

$$z^2 = \frac{s-j}{s}$$

The s -plane squared loss-pole polynomial is

$$P(s)\bar{P}(-s) = (s+j)(-s-j)$$

Since the loss pole at $s = -j1$ transforms to $z^2 = 2$, the squared loss-pole polynomial in the z -plane is

$$P(z)\bar{P}(-z) = (z^2 - 2)^2$$

Choosing only LHP roots for $P(z)$ so as to obtain the maximum number of ripples, we obtain

$$P(z) = (z + \sqrt{2})^2 = z^2 + 2\sqrt{2}z + 2$$

and using Eqn. (24) we get

$$F(z) = z^2 + 2$$

Now the pair of reflection zeros at $z = \pm j\sqrt{2}$ transforms to a single reflection zero at $s = j\frac{1}{3}$. Thus the s -plane reflection-zero polynomial is

$$F(s) = C_f(s - j\frac{1}{3})$$

where the value of the constant C_f determines the passband ripple. For a 3.01 dB ripple we find that $C_f = 3$ (obtained by letting $|K(O)| = F(C)/P(O) = 1$). Finally we use Feldtkeller's equation to obtain the squared natural modes,

$$\begin{aligned} E(s)\bar{E}(-s) &= F(s)\bar{F}(-s) + P(s)\bar{P}(s) \\ &= 9(s - j\frac{1}{3})(-s + j\frac{1}{3}) + (s + j)(-s - j) \end{aligned}$$

$$= 10(s + 0.4 - j0.2)(-s + 0.4 + j0.2)$$

Thus

$$E(s) = \sqrt{10}(s + 0.4 - j0.2),$$

and the transfer function is

$$H(s) = \frac{E(s)}{P(s)} = \sqrt{10} \frac{s + 0.4 - j0.2}{s + j}$$

In conclusion, the z mapping introduced above can be used together with the modified Feldtkeller equation to rewrite filter approximation routines, thus allowing their applicability to the more general case of complex filters. Alternatively, one of the real-to-complex transformations introduced in this section may be used together with existing real-filter approximation programs.

5. Realization

Having solved the approximation problem and thus obtained a suitable complex-coefficient transfer function $T(s)$, the designer must then consider the synthesis problem. In this section we describe a number of approaches for the realization of complex filters. Although our final circuits will be composed of op amps and RC networks, the methods presented are general and can be used to obtain realizations using other technologies, such as the currently popular MOS switched-capacitor circuits.

5.1 Cascade Realization

The first and simplest method we shall present is cascade realization. To

obtain a cascade realization of a complex transfer function $T(s)$, one must first factor $T(s)$ into the product of first-order functions of the general form

$$T_i(s) = \frac{as + b + jc}{s + d + je} \quad (25)$$

Here a, b, c, d and e are real numbers that can be positive, negative or zero; the exception being that d must for stability reasons be positive.

Fig. 14a shows a complex SFG realization of the general first-order complex transfer function of Eqn. (25). This SFG is obtained by realizing the pole using an integrator ($1/s$) with a feedback path having a transmittance $-(d+je)$. The transmission zero is then realized using feedforward. Using the identity of Fig. 3 we obtain the real SFG shown in Fig. 14b. This real SFG can then be used to obtain an active-RC circuit realization following the approach illustrated in Fig. 4.

The circuit realization of an N^{th} order transfer function $T(s)$ is obtained by cascading the N circuit blocks that realize the individual functions in the factorization of $T(s)$. It should be noted, however, that in carrying out a cascade design of a complex filter one is faced with the same problems encountered in the cascade realization of real filters. Specifically, the designer must decide on a pole-zero pairing, on a cascading sequence, and on a distribution of the overall gain among the sections in the cascade. As in real filters, these decisions are usually made in a way that results in the overall filter having the widest possible dynamic range [24].

5.2 Realization Based on a Pole-Forming LC Ladder

Our second realization method is motivated by the desire to obtain low-sensitivity circuits and by the knowledge that doubly-terminated LC ladder networks which are designed for maximum power transfer do have low sensitivities [29]. The method consists of synthesizing a doubly-terminated LC ladder that realizes the poles of the complex filter together with their complex conjugates. An active-RC simulation of this pole-forming network is then obtained. In the active circuit, integrator output voltages simulate the states of the ladder network (that is, its capacitor voltages and inductor currents). The real and imaginary outputs of the complex filter can then be formed as weighted sums of the integrator output voltages. The method is illustrated via the following example.

Example (8)

Let it be required to realize a first-order complex filter having a reflection zero at $s=j1$ and a loss pole at $s=-j0.5$. Feldtkeller's equation [Eqn. (15)] can be used to obtain the squared natural modes, and thus the transfer function is found to be

$$T(s) = \frac{1}{\sqrt{2}} \frac{s + j\frac{1}{2}}{s + \frac{3}{4} - j\frac{1}{4}} \quad . \quad (26)$$

Multiplying numerator and denominator by the polynomial containing the complex conjugate of the pole yields

$$T(s) = \frac{1}{\sqrt{2}} \frac{(s^2 + \frac{3}{4}s - \frac{1}{8}) + j(\frac{3}{4}s + \frac{3}{8})}{s^2 + \frac{3}{2}s + \frac{5}{8}} \quad (27)$$

Thus the pole-forming LC ladder must have the natural mode polynomial $(s^2 + \frac{3}{2}s + \frac{5}{8})$. Obviously, however, there is some choice in the selection of a ladder network since its transmission and reflection zeros are not specified. For the purposes of this example we shall use the low-pass ladder of Fig. 15a which has the voltage transfer function

$$\frac{V_C(s)}{V_i(s)} = \frac{1/3.2}{s^2 + \frac{3}{2}s + \frac{5}{8}} \quad (28)$$

This ladder has two state variables: the capacitor voltage V_C , given by Eqn. (26), and the inductor current I_L given by

$$\frac{I_L(s)}{V_i(s)} = \frac{\frac{1}{4}s + \frac{1}{3.2}}{s^2 + \frac{3}{2}s + \frac{5}{8}} \quad (29)$$

The real and imaginary parts of the transfer function in (27) can be formed as weighted sums of the two state variables V_C and I_L in Eqns. (28) and (29) as follows.

$$T_R(s) = \frac{1}{\sqrt{2}} + \frac{0.6}{\sqrt{2}} \frac{V_C(s)}{V_i(s)} - \frac{3}{\sqrt{2}} \frac{I_L(s)}{V_i(s)} \quad (30)$$

$$T_I(s) = -\frac{1.8}{\sqrt{2}} \frac{V_C(s)}{V_i(s)} + \frac{3}{\sqrt{2}} \frac{I_L(s)}{V_i(s)} \quad (31)$$

Using standard techniques [24] we obtain the active-RC circuit in Fig. 15b that simulates the operation of the pole-forming ladder of Fig. 15a. This cir-

cuit includes two summing op amps which implement the weighted summations of Eqns. (30) and (31) and thus form the real and imaginary outputs of the complex filter. Finally, note that this realization of the complex filter assumed that the input is a real signal. If this is not the case, the circuit can be augmented to allow for the imaginary input.

Further details on this realization method have been given elsewhere [19].

5.3 Realization Based on the Simulation of a Doubly-Terminated LCX

Ladder

The above realization method, though it yields good results, does not result in circuits with very low sensitivities. This is because the pole-forming ladder does not have maximum power transfer in the passband of the complex filter. To obtain a realization that takes full advantage of the low-sensitivity properties of LC ladders one must first synthesize a doubly-terminated ladder that realizes the complex transfer function $T(s)$. To be able to do so we shall include a new component, *the imaginary-valued resistance*. This is an element having the impedance jX where X is a constant (positive or negative)*.

With the inclusion of the lossless jX element one can synthesize lossless LCX ladder networks that can be doubly terminated and designed to deliver maximum power to the load over the passband of the complex filter. An active-RC realization of the complex filter can then be obtained using a signal flow graph simulation of the operation of its LCX ladder realization.

* The imaginary resistance differs from the pure reactance used by Humpherys [9] in that the pure reactance displays odd symmetry with respect to ω .

A full theory for the synthesis of LCX networks will not be presented here. Rather, we shall present sufficient material to enable the design of a variety of complex filters using the LCX technique.

The imaginary-valued resistance jX is a one-port network defined in the time domain by

$$v(t) = jX\hat{i}(t) \quad (32)$$

and in the frequency domain by

$$V(j\omega) = jXI(j\omega) \quad (33)$$

Fig. 16a shows the circuit symbol for the imaginary-valued resistance (note that the symbol is that of a real-valued resistance rotated 90°). Fig. 16b shows the complex SFG representation of the operation of the imaginary-valued resistance. The real SFG equivalent is shown in Fig. 16c.

Expressing $V(j\omega)$ and $I(j\omega)$ in Eqn. (33) in terms of their real and imaginary parts yields the following pair of equations which describe the operation of the imaginary-valued resistance:

$$V_R(j\omega) = -XI_I(j\omega) \quad (34)$$

$$V_I(j\omega) = XI_R(j\omega) \quad (35)$$

This description suggests that the one-port imaginary-valued resistance can be realized by the real two-port network shown in Fig. 17a. This network can be recognized as the realization of a gyrator having a gyration resistance of X ohms, as shown in Fig. 17b. The equivalence of the imaginary-valued resistance to the ideal gyrator confirms the fact that it is indeed a lossless element.

To gain further insight into LCX networks consider the CX tank circuit shown in Fig. 18a. One can show that the operation of this tank circuit is described by the SFG shown in Fig. 18b. Also, the CX tank is equivalent to the capacitively terminated ideal gyrator shown in Fig. 18c. Note that the "real" equivalent circuit in Fig. 18c uses a gyrator to represent X and a pair of capacitors to represent C : one capacitor stores "real" charge and the other "imaginary" charge. Now, because the impedance of the CX tank is

$$Z(s) = \frac{1}{sC - j\frac{1}{X}}$$

it has a natural mode on the $j\omega$ axis and thus oscillates at a frequency $\frac{1}{CX}$. In fact, it is easy to see that the equivalent gyrator circuit in Fig. 18c is a quadrature oscillator. Finally, note that because the CX tank exhibits infinite impedance at $s = j\frac{1}{XC}$, it can be used to create transmission zeros in ladder networks just as we use LC tanks in "real" LC ladders.

Fig. 19 provides another illustration of the realization of RLCX networks by RLC-gyrator circuits*. Although these equivalences are theoretically interesting, our complex filters will be realized using SFG operational simulation techniques.

We next consider the synthesis of doubly terminated LCX filters. The synthesis process involves the same major steps as for real LC networks [24]: reduction of the two-port problem to a one-port synthesis; a series of full and partial (or zero-shifting) removals; and calculation of the termination impedance.

* It is fascinatingly similar in appearance to some linear-phase filters discussed by Rhodes [31], except that inputs and outputs are differently arranged.

We approach the reduction to one-port problem in a non-traditional way. The reflection coefficient at the input of a doubly-terminated two-port network is given by

$$\rho(s) = \frac{Z_{in}(s) - R_s}{Z_{in}(s) + R_s} \quad (36)$$

where R_s is the source resistance and $Z_{in}(s)$ is the input impedance. We can use (36) to express the input impedance as

$$Z_{in}(s) = R_s \frac{1 + \rho(s)}{1 - \rho(s)} \quad (37)$$

where $\rho(s)$ can be expressed as the ratio of the reflection-zero polynomial $F(s)$ to the natural mode polynomial $E(s)$,

$$\rho(s) = \frac{F(s)}{E(s)} \quad (38)$$

From the given $\rho(s)$ we find $Z_{in}(s)$ using (37) and carry out the synthesis by choosing a topology with the appropriate $P(s)$ and perform removal operations from $Z_{in}(s)$, thus determining the element values. We shall illustrate the process by an example.

Example (9)

Let it be required to find a doubly-terminated LCX realization of a first-order complex filter having $P(s) = s - j$ and $F(s) = s + j$. Using Feldtkeller's equation we find that $E(s) = \sqrt{2}(s + 1)$. Using (37) and assuming $R_s = 1\Omega$ we find $Z_{in}(s)$ to be

$$Z_{in}(s) = \frac{\sqrt{2}(s+1)+s+j}{\sqrt{2}(s+1)-s-j} \quad (39)$$

We need a first-order network with a loss pole at $s=j$. This loss pole can be implemented with a shunt tank or a series tank, using an LX or a CX. These four possible tank circuits are shown in Fig. 20.

We also need a partial removal, because the tank circuits of Fig. 20 have either 0 or ∞ impedance at $s=j$ while

$$Z_{in}(s)|_{s=j} = j(\sqrt{2}+1)$$

Thus our network must contain either a $j(\sqrt{2}+1)$ ohms shunt resistor followed by a series-arm tank or a $j(\sqrt{2}+1)$ ohm series resistance followed by a shunt-arm tank. If we decide to start with the series X , we can get a new synthesis impedance $Z_2(s)$ by "removing" X , (see Fig. 21a)

$$Z_2(s) = Z_{in}(s) - j(\sqrt{2}+1)$$

$$= \frac{(\sqrt{2}+1)s-1-j(s+\sqrt{2}+1)}{\sqrt{2}(s+1)-s-j}$$

which as expected has a zero at $s=j$.

Next we can perform a full removal of an LX or a CX tank resonant at $s=j$. The impedance of the LX tank (see Fig. 21b) is $Z(s) = sL + jX = L(s + j\frac{X}{L})$. It follows that $\frac{X}{L} = -1$. The value of L can be found from

$$\lim_{s \rightarrow j} Z_2(s) = L(s-j)$$

which yields $L = (1 + \frac{1}{\sqrt{2}})H$ and $X = -(1 + \frac{1}{\sqrt{2}})\Omega$.

The next step involves determining the remainder impedance $Z_3(s)$ (see

Fig. 21b).

$$Z_3(s) = 1 / \left[\frac{1}{Z_2(s)} - \frac{1}{Z(s)} \right] = 3 + 2\sqrt{2} - j(1 + \sqrt{2})$$

This is a series combination of an imaginary-valued resistor $[-j(1 + \sqrt{2})]$ and a load resistance of $(3 + 2\sqrt{2})\Omega$. This completes the synthesis process and the resulting LCX network is that shown in Fig. 21c.

Once an LCX realization is obtained, it is a straightforward matter to find an active-RC implementation. Firstly, a complex SFG that simulates the operation of the LCX network is found following procedures identical to those employed in the operational simulation of LC ladders. Secondly, the identity of Fig. 3 is used to obtain a real SFG. Finally, an active-RC circuit realization of the real SFG is obtained.

As a practical example we show in Fig. 22 the LCX realization of the second-order complex filter whose transfer function was obtained in Example (3) and whose theoretical magnitude and phase responses are shown in Fig. 10. A single (real)-input active-RC realization of this filter is shown in Fig. 23. This circuit was constructed [30] and its frequency response was measured using a set up based on the discrete Fourier transform*. The measured response is shown in Fig. 24.

* This technique for measuring the frequency response of complex filters will be reported in the near future. Essentially the two real transfer functions $T_R(j\omega)$ and $T_I(j\omega)$ may be measured and combined mathematically to obtain $T(j\omega) = T_R(j\omega) + jT_I(j\omega)$.

5.4 A Realization Method for Arithmetically-Symmetric Complex

Bandpass Filters

We shall conclude this section by presenting a simple method for the realization of arithmetically-symmetric complex bandpass filters. The method is based on the transformation $p = s - j\omega_0$ employed in Section 4.2 to obtain a suitable transfer function $T(s)$ (refer to Fig. 11). The effect of this transformation on the elements of an LC ladder realization of the real low-pass prototype (that is, that with the attenuation specifications shown in Fig. 11b) is illustrated in Fig. 25. It follows that by simply applying this transformation to the LC realization of the real low-pass prototype we obtain an LCX realization of the complex bandpass filter.

Once an LCX realization is found, an active-RC simulation of its operation can be obtained in the usual manner. However, a simpler alternative is available here: We first obtain an active-RC simulation of the real prototype filter. Next, we apply the transformation $p = s - j\omega_0$ to the active-RC circuit. The result will simply be that each integrator $1/p\tau$ will be replaced by a complex integrator $1/(s - j\omega_0)\tau$, as shown in Fig. 26. This complex integrator can in turn be realized in the manner illustrated in Fig. 27. It follows that the realization of the complex bandpass filters will consist of two identical real filters, each of which is a realization of the real low-pass prototype, with each pair of corresponding integrators coupled via $-\omega_0\tau$, $\omega_0\tau$ links as shown for the integrator in Fig. 27. It is interesting to note that by varying the transmittances of these links (that is, varying the values of the coupling resistors in the actual circuit) we are able to shift the response of the complex filter along

the ω axis. We have used this realization method to design and construct a tunable sixth-order complex bandpass filter and obtained good experimental results. Another eighth-order complex bandpass filter with very stringent specifications was also designed and constructed using this approach.

6. Conclusions

We have provided approximation and realization methods for the design of analog filters having complex-valued coefficients. It is hoped that these relatively simple methods will increase the attractiveness of this useful class of linear analog filters. However, a number of important problems need further investigation. These include: a fuller study of the LCX realization, a study of the sensitivity of the various realizations (especially from the point of view of differential changes between the real and imaginary outputs), development of techniques for measuring the response of complex filter, and, perhaps most importantly, finding novel applications for complex filters. Preliminary results on a number of these problems will be reported in the near future.

Figure Captions

- Fig. 1 Magnitude response (b) and phase response (c) of the first-order complex filter having the single complex pole shown in (a).
- Fig. 2 (a) Black-box representation of a complex analog filter $T(s)$. (b) Representation of $T(s)$ as a complex signal flow graph (SFG). (c) Block-diagram realization of the complex filter. (d) Representation of the realization in (c) as a real SFG.
- Fig. 3 Relationship between a complex SFG and its real equivalent.
- Fig. 4 Realization of the complex transfer function $T(s) = -1/(s+1-j)$: (a) complex SFG, (b) real SFG obtained using the identity of Fig. 3, and (c) op-amp circuit implementation of the SFG in (b).
- Fig. 5 The phase-shift method for generating SSB signals.
- Fig. 6 (a) Direct generation of SSB signal using complex filter. (b) Implementation of the SSB modulator in (a).
- Fig. 7 (a) Spectrum of a bandpass signal. (b) Multiplying the bandpass signal in (a) by $e^{-j\omega_c t}$ results in a complex baseband signal-together with the signal at $-2\omega_c$. The latter can be eliminated by the real low-pass filter indicated, as shown in Fig. 8.
- Fig. 8 (a) Implementation of the demodulation, low-pass filtering and sampling of a bandpass signal. (b) the real equivalent.
- Fig. 9 An alternative approach to the sampling of bandpass signals. A complex bandpass filter is employed obviating the need for demodulation.

Fig. 10 Computed attenuation and phase characteristics of the second-order complex filter of Example 3.

Fig. 11 Approximation for the arithmetically-symmetric bandpass filter specifications in (a) is obtained by first shifting the specifications linearly along the frequency axis, obtaining a "real" approximation for the shifted specifications (b), and then shifting the resulting function by $j\omega_0$ (c).

Fig. 12 Illustrating the application of the transformation $s = p^2/j$ to obtain an approximation to the specifications of a complex SSB filter (Example 5).

Fig. 13 The mapping of Eqn. (18) transforms the specifications in (a) to those in (b) which extend only over the positive frequency axis.

Fig. 14 (a) Complex SFG realization of the general first-order complex transfer function of Eqn. (25). (b) Real SFG equivalent.

Fig. 15 (a) A doubly-terminated LC ladder realization of the natural modes (and their conjugates) of the complex filter of Example (8). (b) An active-RC simulation of the operation of the ladder in (a) with the real and complex outputs of the complex filter formed as weighted sums of the state-variables.

Fig. 16 The imaginary-valued resistance (a), its complex SFG representation (b), and the real SFG representation (c).

Fig. 17 Realization of an imaginary-valued resistance as a real gyrator.

Fig. 18 A CX tank (a), its SFG representation (b), and its gyrator-C realization.

- Fig. 19 An RLCX circuit (a) and its RLC-gyrator realization (b).
- Fig. 20 Four possible tank circuits for the realization of a single $j\omega$ -axis loss pole in the synthesis of LCX ladder networks.
- Fig. 21 Illustrating the synthesis of a doubly-terminated LCX ladder reauization for the first-order complex filter of Example (9).
- Fig. 22 A doubly-terminated LCX ladder realization of the second-order complex bandpass filter of Example (3). This realization is frequency normalized to 1 kHz.
- Fig. 23 Active-RC implementation of the second-order complex bandpass filter whose LCX ladder realization is shown in Fig. 22. All resistances are in $k\Omega$.
- Fig. 24 Measured frequency response of the complex bandpass filter of Fig. 23.
- Fig. 25 Application of the transformation $p = s - j\omega_0$ to elements of the LC realization of a real low-pass prototype.
- Fig. 26 Application of the transformation $p = s - j\omega_0$ to an integrator in the active-RC simulation of the operation of a low-pass prototype realization.
- Fig. 27 Realization of a complex integrator as a pair of coupled real integrators.

References

- [1] D. Gabor, "Theory of communication", Proc. IEE, vol. 93, pt. 3, pp. 429-457, Nov. 1946.
- [2] E. Bedrosian, "The analytic signal representation of modulated waveforms", Proc. IRE, pp. 2071-2076, Oct. 1962.
- [3] R.F. Baum, "Design of unsymmetrical bandpass filters", IRE Trans. Circuit Theory, vol. CT-4, pp. 33-40, June 1957.
- [4] V. Belevitch, Classical Network Theory, Holden-Day, San Francisco, 1968.
- [5] H.B. Voelcker, "Toward a unified theory of modulation - Part I: Phase-envelope relationships", Proc. IEEE, vol. 54, pp. 340-353, March 1966 and "Part II: Zero manipulation", Proc. IEEE, vol. 54, pp. 735-755, May 1966.
- [6] W.R. Bennett, Introduction to Signal Transmission, McGraw-Hill, New York, 1970.
- [7] Y. Fang, "New methods to generate vestigial-sideband signal for data transmission", IEEE Trans. on Communications, vol. COM-20, pp. 147-157, April 1972.
- [8] E.S. Kuh and R.A. Rohrer, Theory of Linear Active Networks, Holden-Day, San Francisco, 1967.
- [9] D.S. Humphreys, The Analysis, Design and Synthesis of Electrical Filters, Prentice-Hall, Englewood Cliffs, N.J., 1970.
- [10] S. Haykin, Communication Systems, Wiley, New York, 1978.
- [11] G.R. Lang and P.O. Brackett, "Baseband and passband equalizers for linear modulation systems", Proc. 1972 IEEE Int. Symp. on Circuit

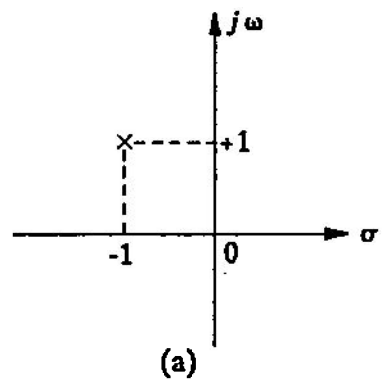
- Theory, pp. 96-100, North Hollywood, Calif., April 1972.
- [12] A. Fettweis, "Complex wave digital filters", Proc. 1980 IEEE Int. Symp. on Circuits and Systems, Houston, April 1980.
- [13] K. Meerkotter, "Complex passive networks and wave digital filters", Proceedings of the 1980 European Conference on Circuit Theory & Design, pp. 24-35, Warsaw, Poland, Sept. 1980.
- [14] M.T. McCallig, "Design of FIR filters with complex conjugate pulse responses", IEEE Trans. on Circuits and Systems, vol. CAS-25, pp. 1103-1105, Dec. 1978.
- [15] M.J. Gingell, "Single sideband modulation using sequence asymmetric polyphase networks", Electrical Communications, vol. 48, No. 1 and 2, pp. 21-25, 1973.
- [16] W.F. McGee, "The analysis and synthesis of modulator filters using symmetrical components", Proceedings of the Second International Symposium on Large Engineering Systems, pp. 15-22, Waterloo, Canada, May 15, 16, 1978.
- [17] E. Daoud, W.B. Mikhael and M.N.S. Swamy, "New active-RC networks for the generation and detection of single-sideband signals", IEEE Trans. on Circ. and Systs., vol. CAS-27, pp. 1140-1154, Dec. 1980.
- [18] T. Tsuchiya and S. Shida, "On the design of broadband 90-degree phase splitting networks", IEEE Trans. on Circuits and Systems, vol. CAS-27, pp. 30-36, Jan. 1980.
- [19] G.R. Lang and P.O. Brackett, "Complex analog filters", Proc. of the 1981 European Conference on Circuit Theory and Design, pp., The Hague, The

Netherlands, Sept. 1981.

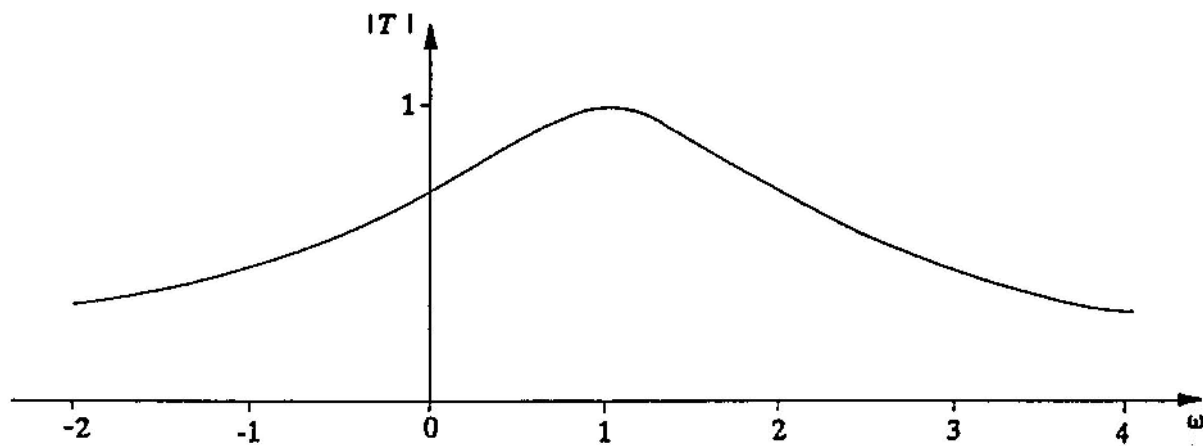
- [20] W.M. Snelgrove and A.S. Sedra, "State-space synthesis of complex analog filters", Proc. 1981 European Conference on Circuit Theory and Design, pp., The Hague, The Netherlands, Sept. 1981.
- [21] D.E. Norgaard, "The phase-shift method of single-sideband signal generation", Proc. IRE, vol. 44, pp. 1719-1735, Dec. 1956.
- [22] A.V. Oppenheim and R.W. Schafer, Digital Signal Processing, Prentice Hall, Englewood Cliffs, N.J., 1975.
- [23] R.W. Daniels, Approximation Methods for Electronic Filter Design, McGraw-Hill, New York, 1974.
- [24] A.S. Sedra and P.O. Brackett, Filter Theory and Design: Active and Passive, Matrix, Portland, Oregon, 1978.
- [25] G.R. Lang, "Easy - an advanced design program for analog and digital filters", Proc. 1973 IEEE Int. Symp. on Circuit Theory, Toronto, Canada, 1973.
- [26] W.F. McGee, "Numerical approximation technique for filter characteristic functions", IEEE Trans. on Circuit Theory, vol. CT-14, pp. 92-94, March 1967.
- [27] H.J. Orchard and G.C. Temes, "Filter design using transformed variables", IEEE Trans. Circuit Theory, vol. CT-15, pp. 385-405, 1968.
- [28] W.M. Snelgrove, "FILTOR-2: A computer-aided filter design program". Dept. of Electrical Engineering, University of Toronto, Toronto, Canada, 1981.
- [29] H.J. Orchard, "Inductorless filters", Electron. Lett., vol. 2, pp. 224-225,

June 1966.

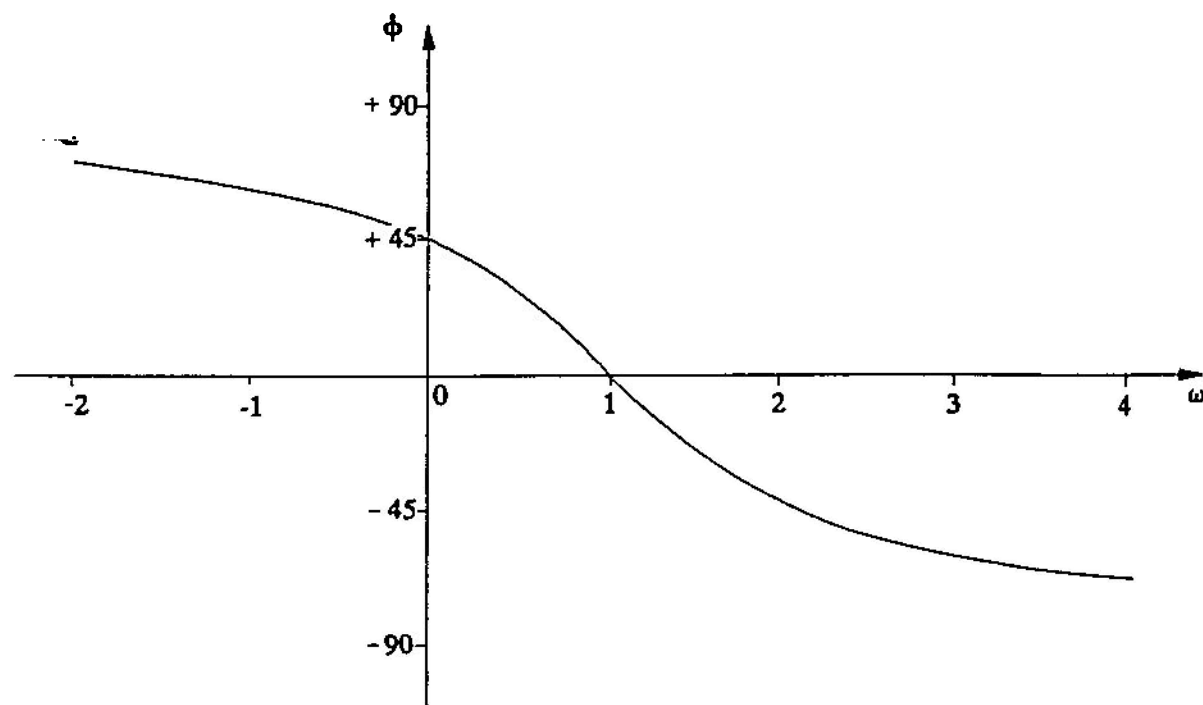
- [30] Lillian Diaz Olavarieta, State-Space Synthesis of Analog Complex Filters, M.Sc. Thesis, INAOE, Mexico, 1982.
- [31] J.D. Rhodes, Theory of Electrical Filters, John Wiley and Sons, 1976.



(a)



(b)



(c)

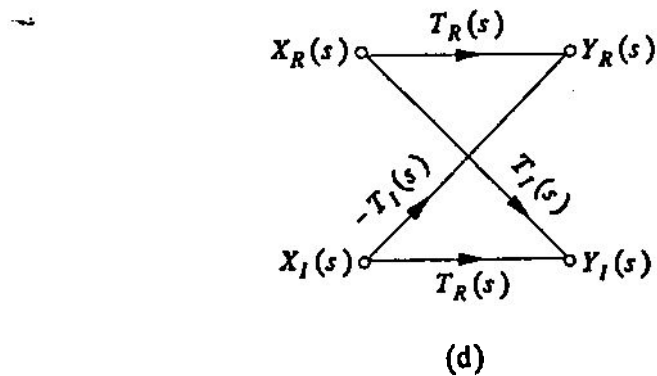
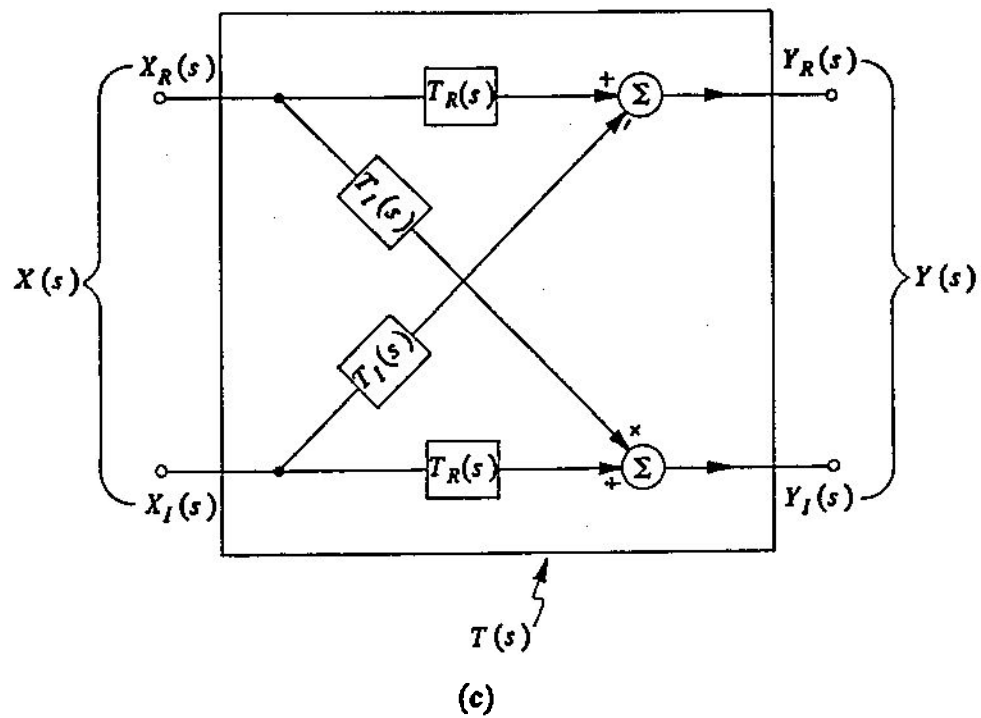
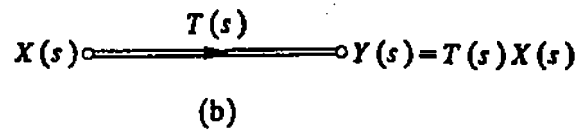
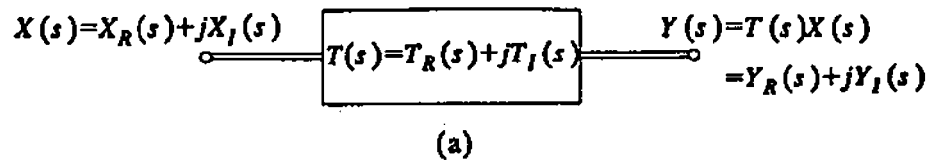


Fig. 2

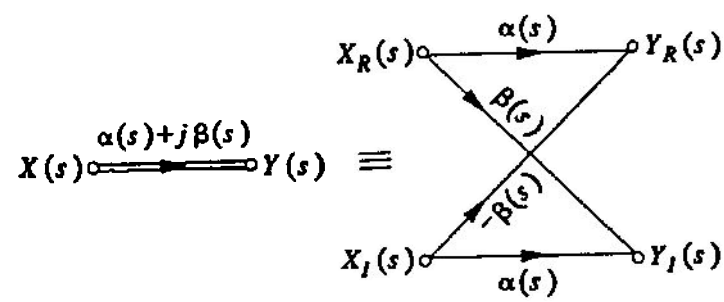
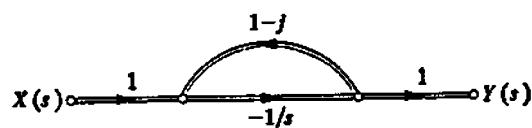
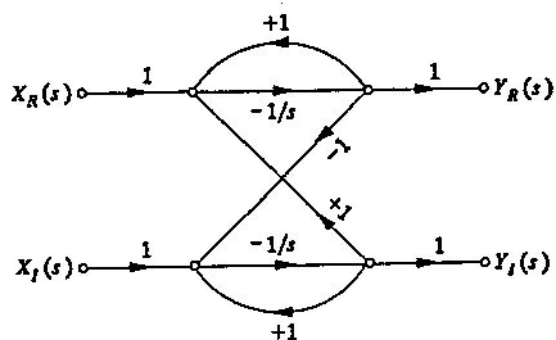


Fig. 3



(a)



(b)

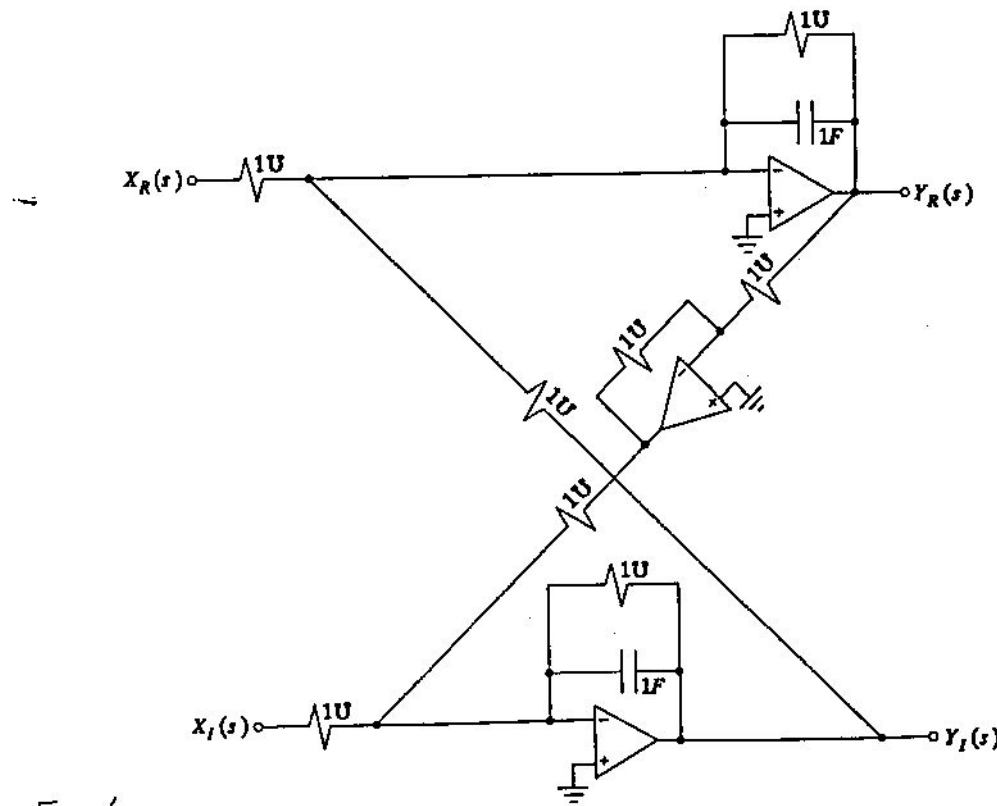


Fig. 4

(c)

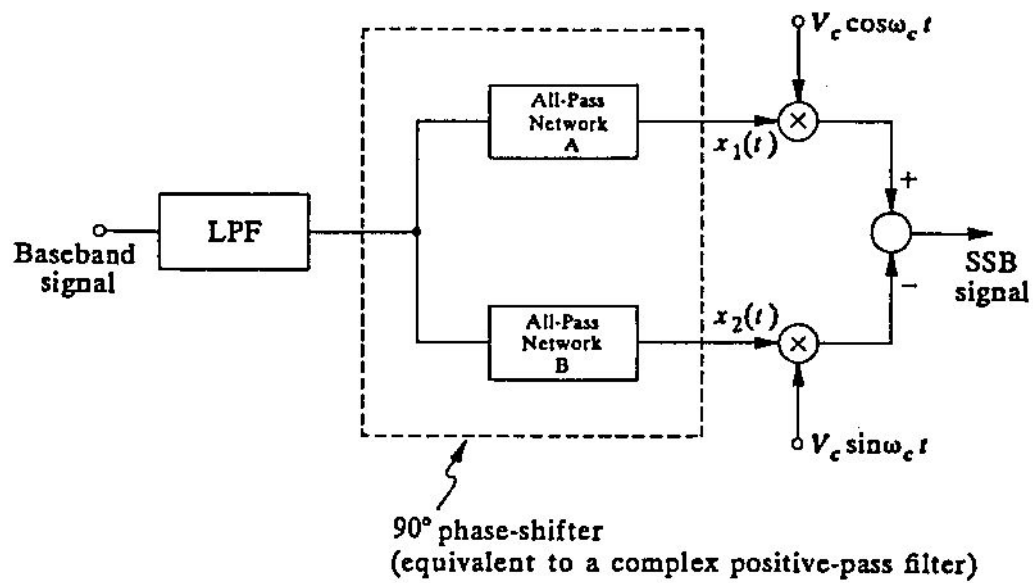
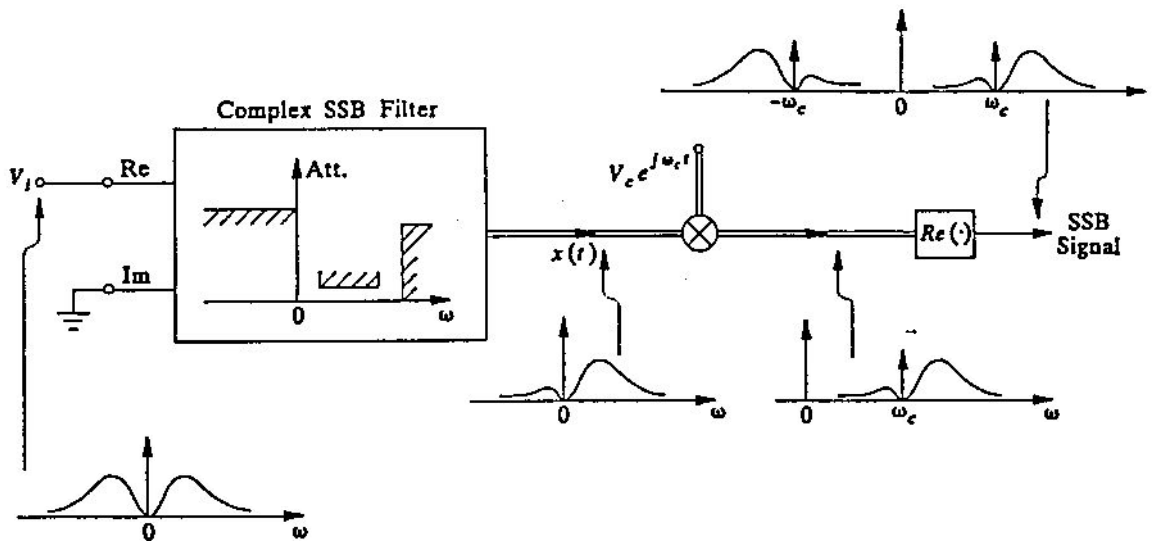
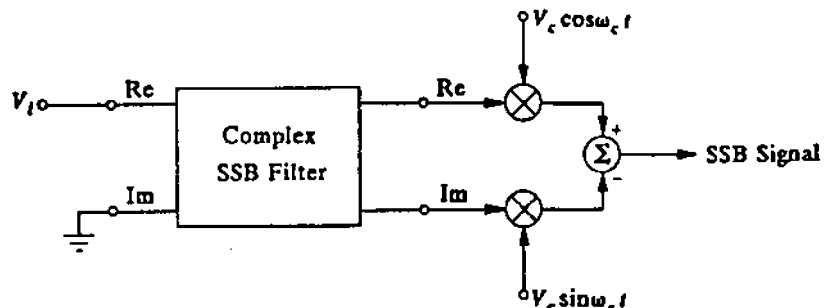


Fig. 5



(a)



(b)

Fig. 6

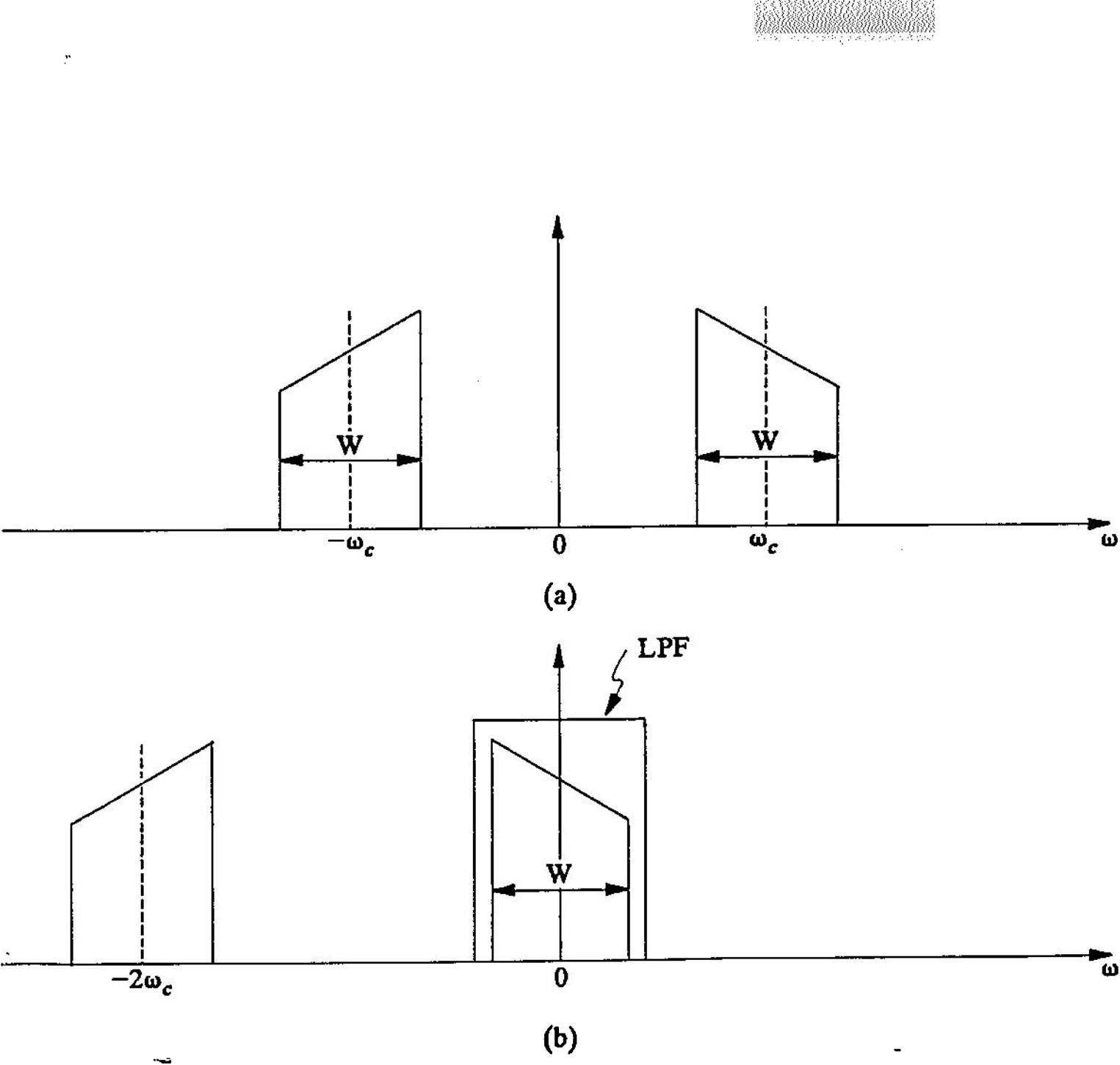
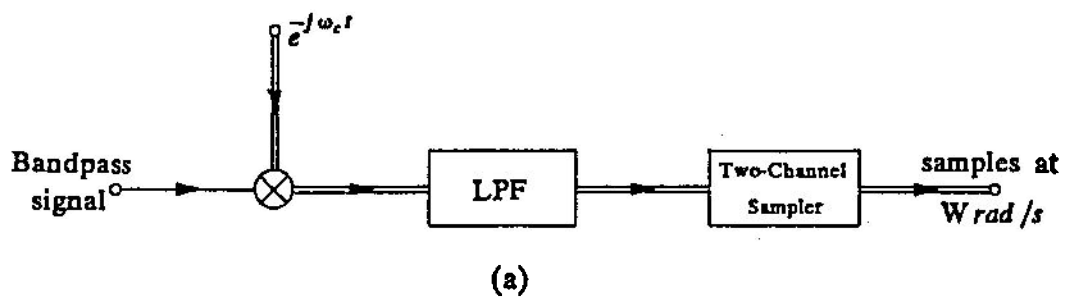
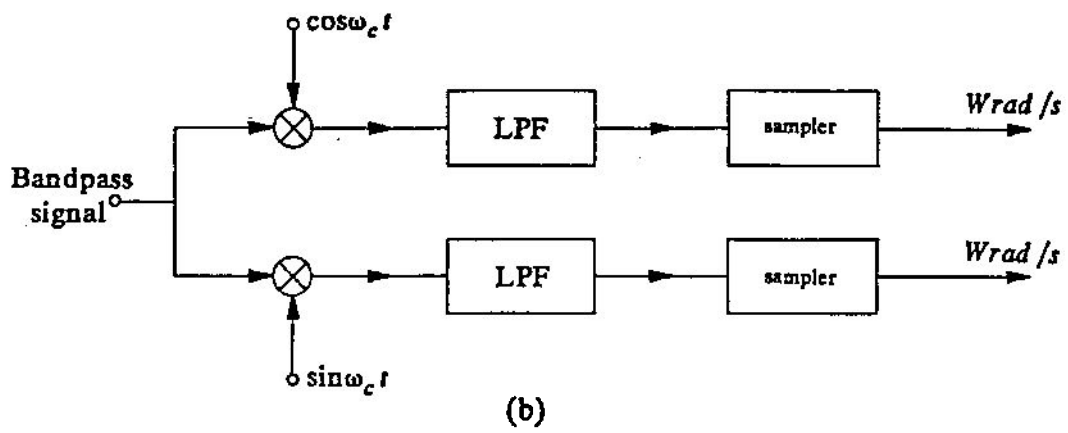


Fig. 7



(a)



(b)

Fig. 8

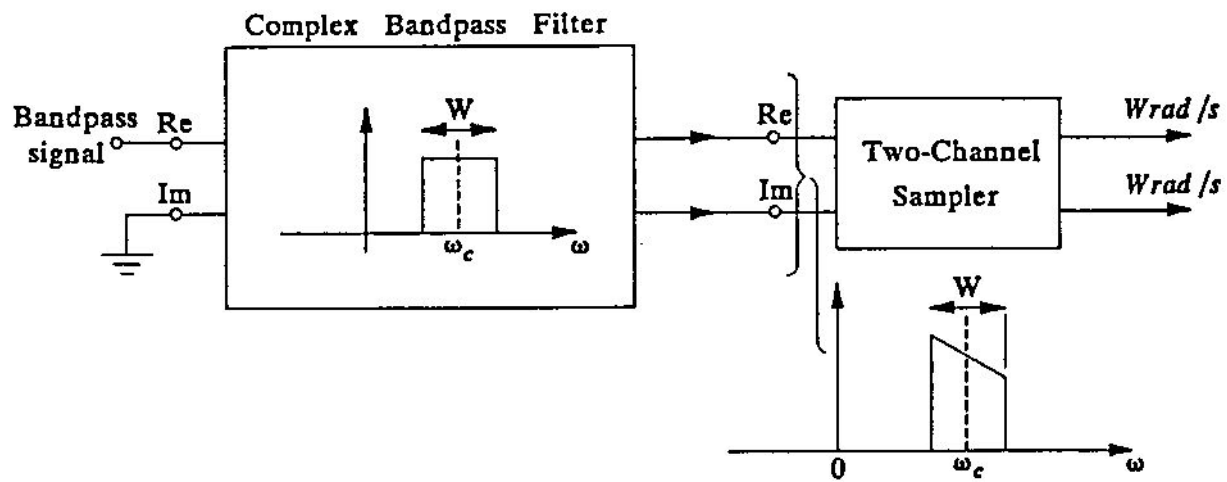


Fig. 9

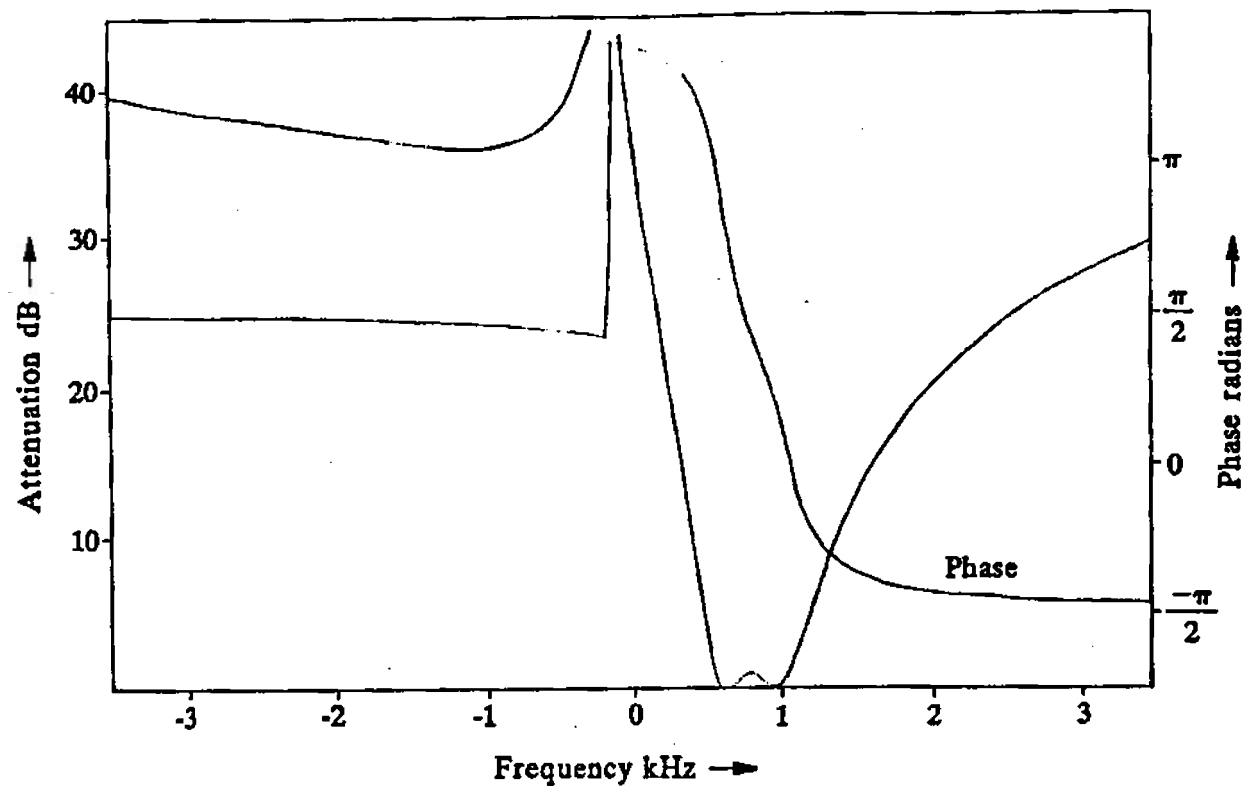


Fig 10

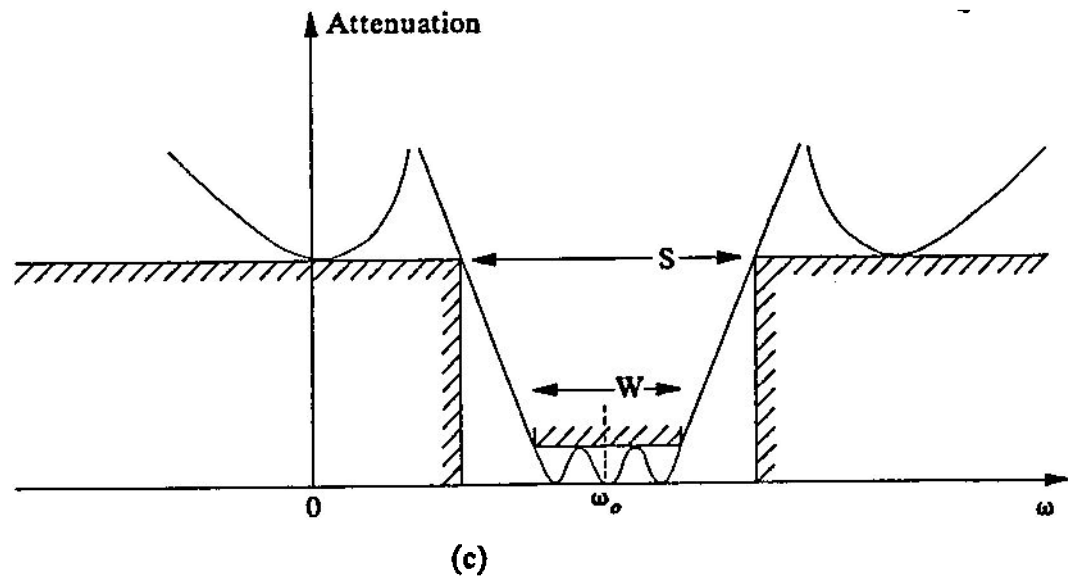
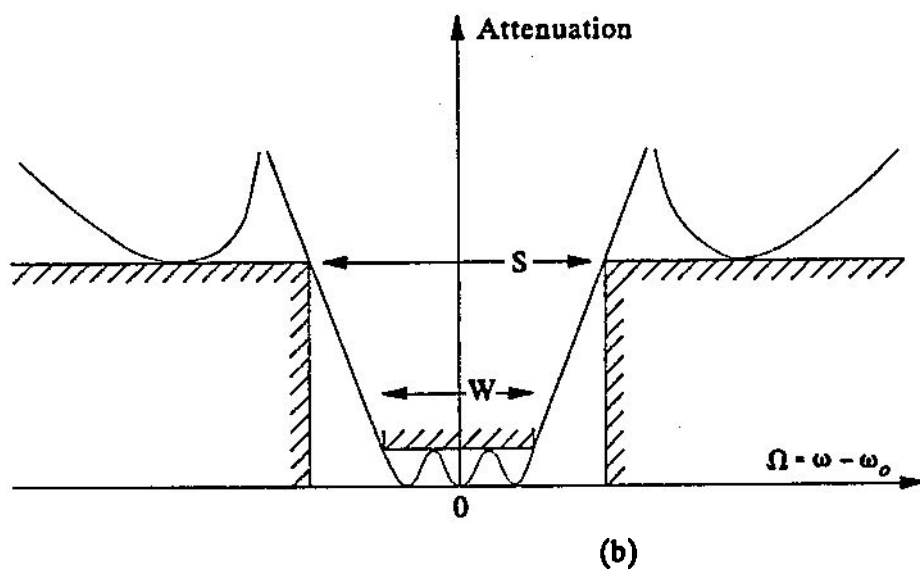
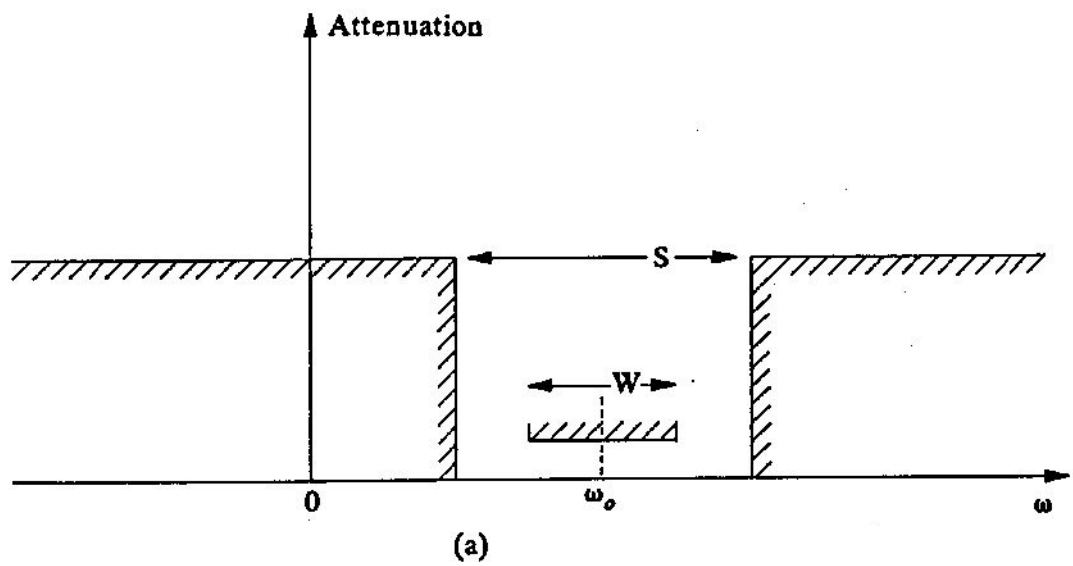
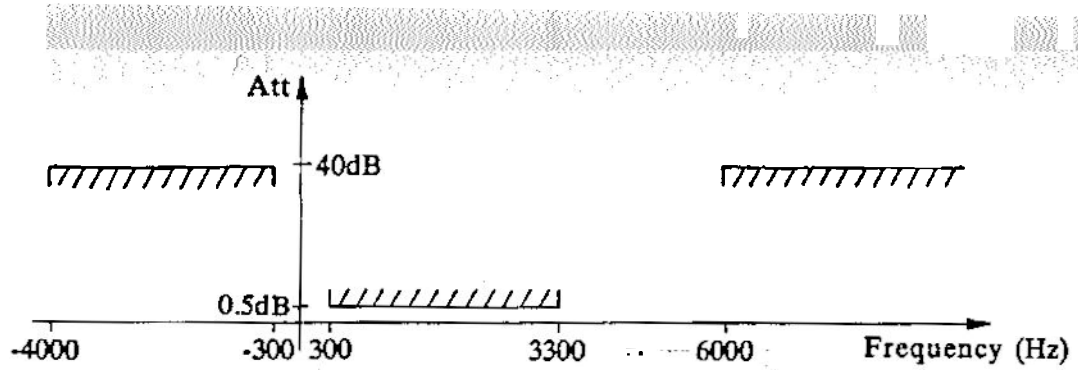
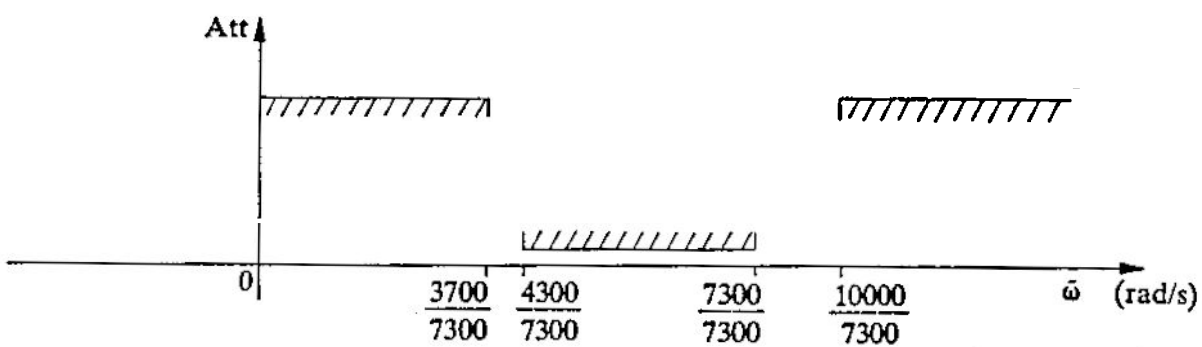


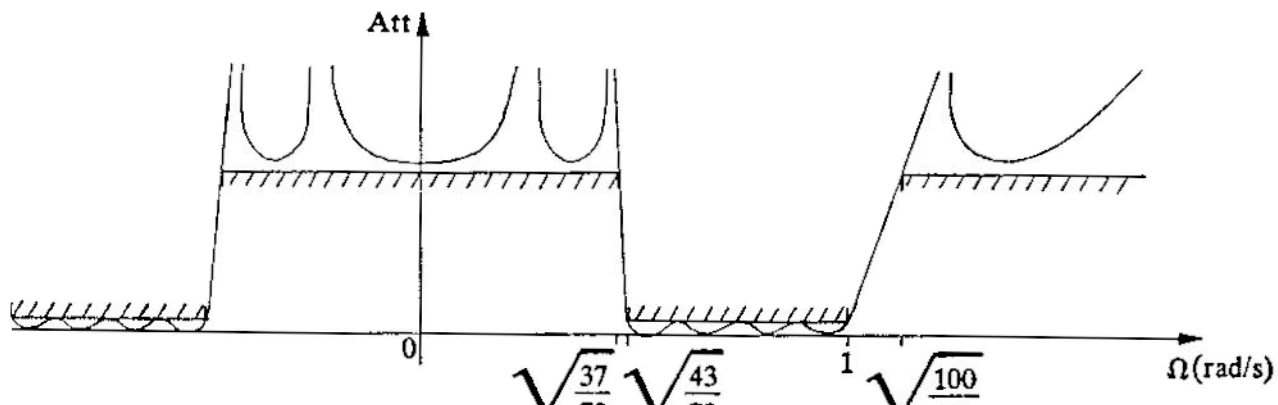
Fig. 11



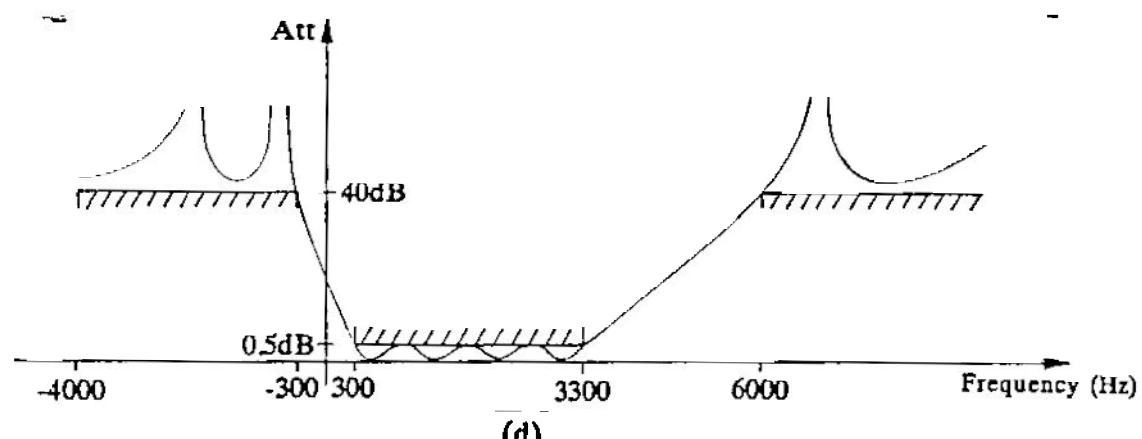
(a)



(b)



(c)



(d)

Fig 12

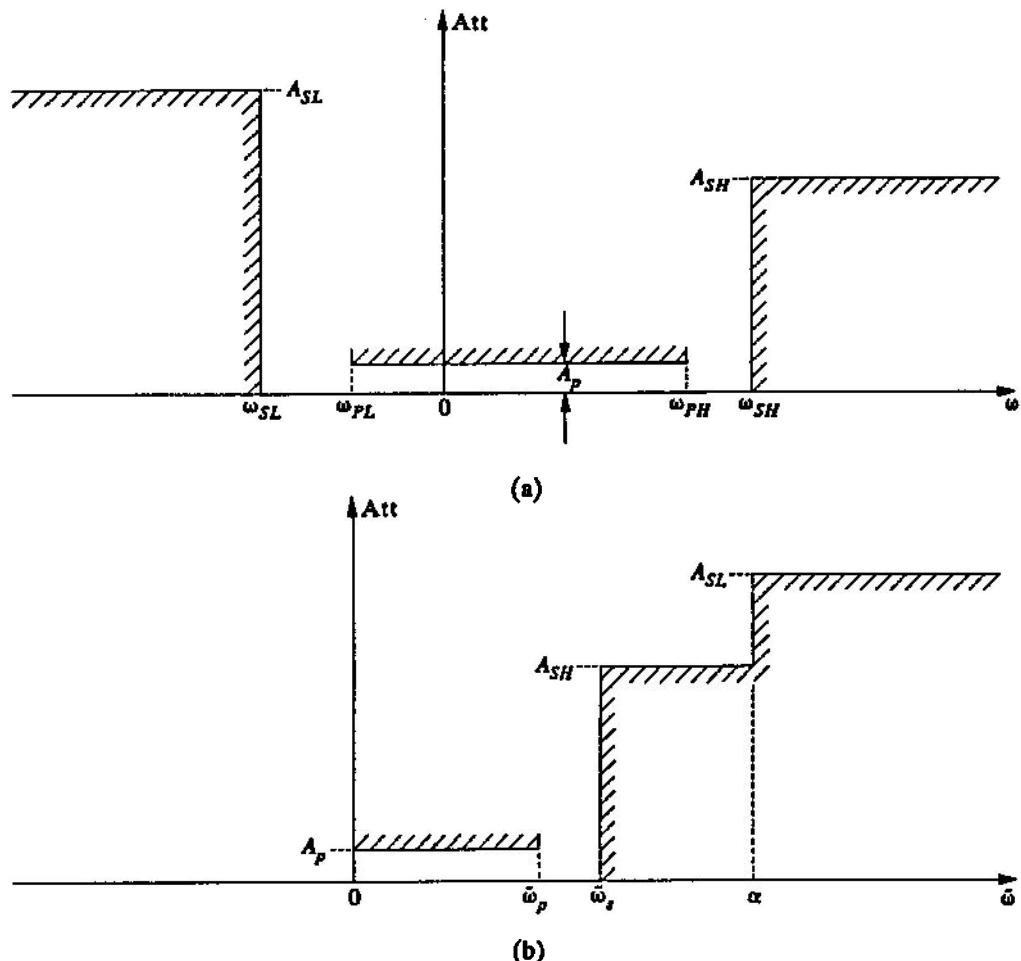
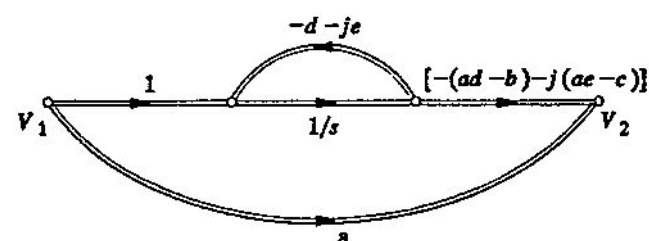
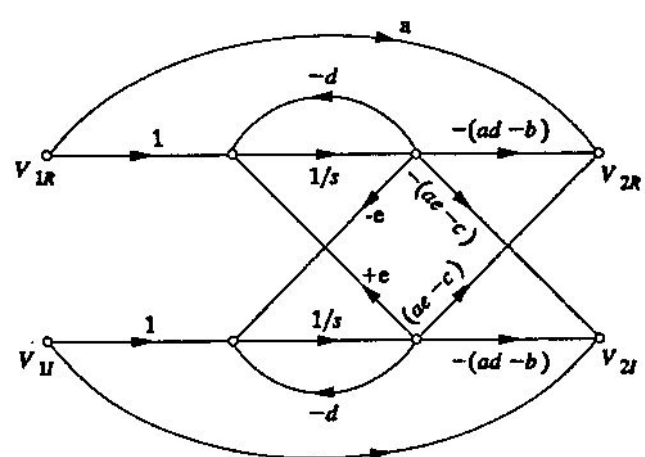


Fig. 13

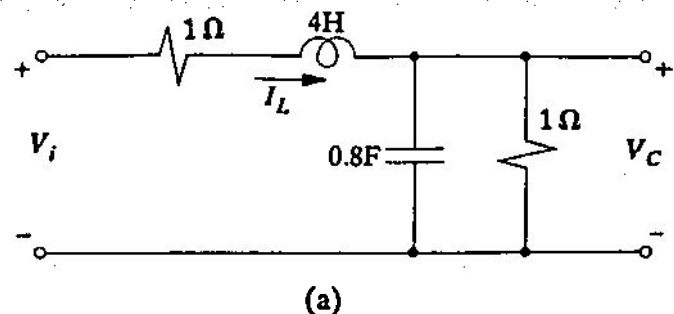


(a)

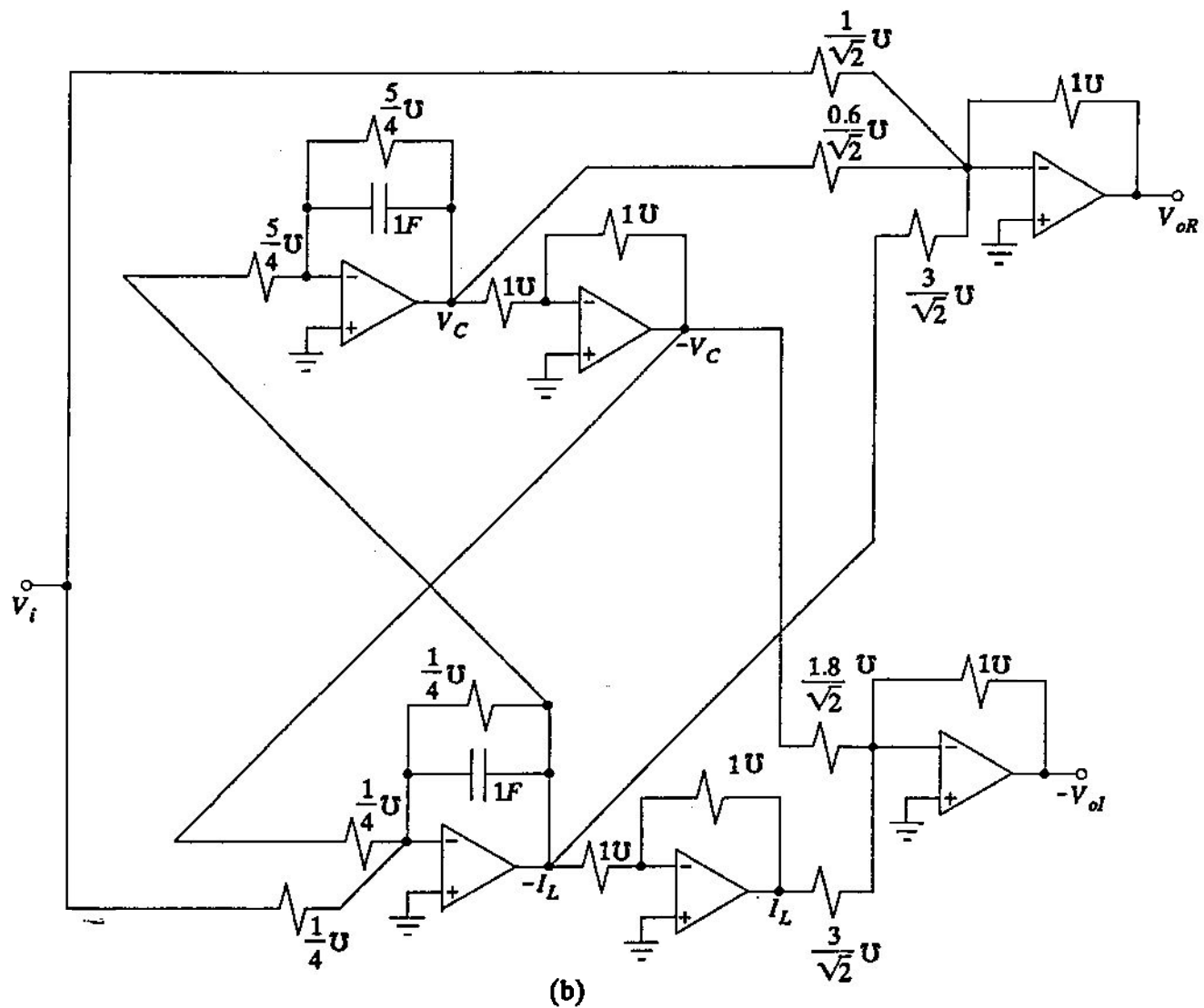


(b)

Fig. 14



(a)



(b)

Fig 15

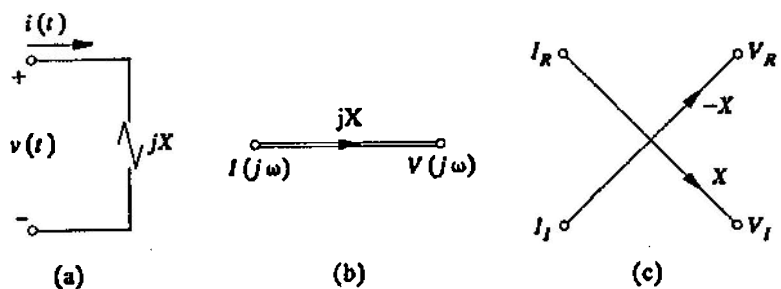


Fig 16.

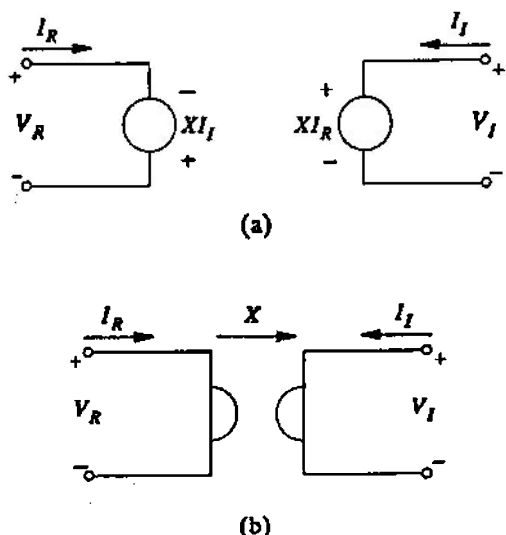


Fig 17

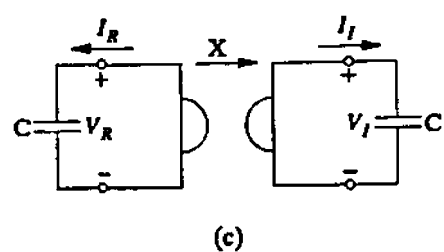
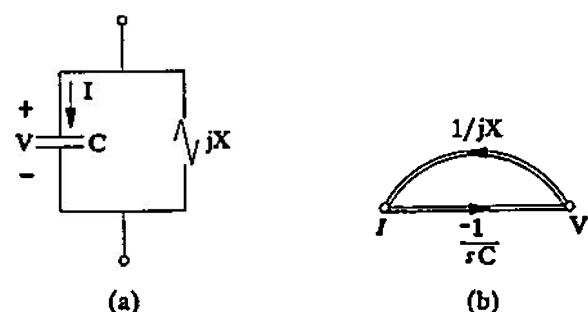
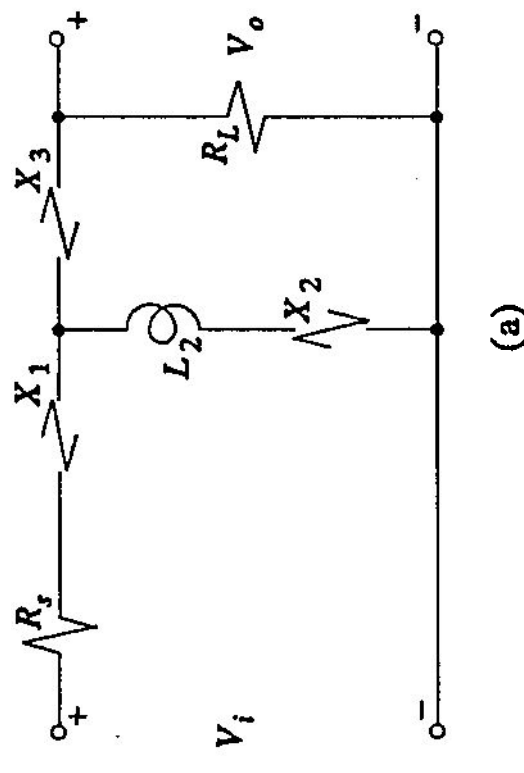
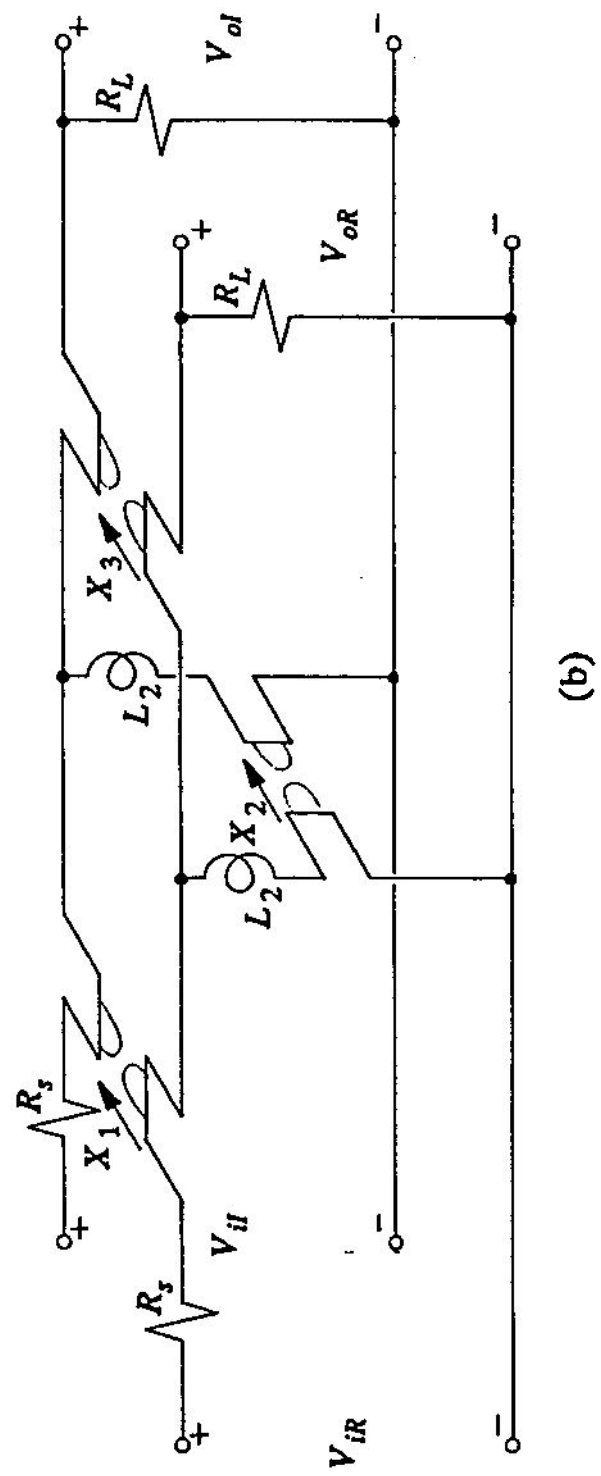


Fig 18



(a)



(b)

Fig. 19

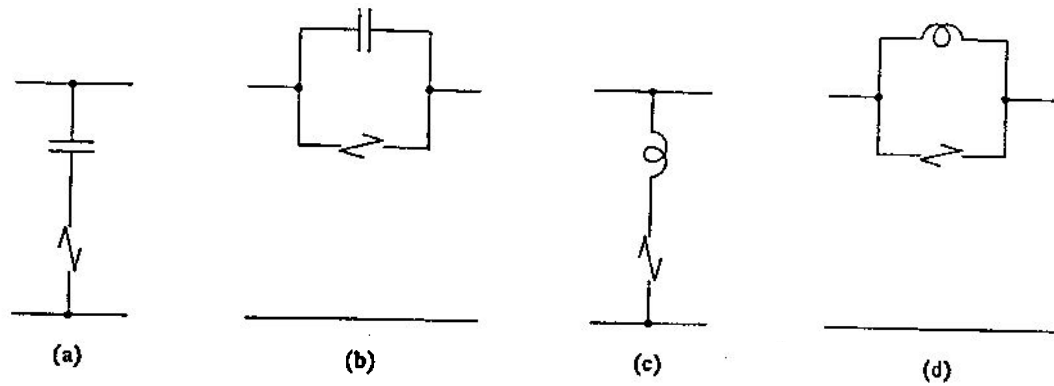


Fig. 20

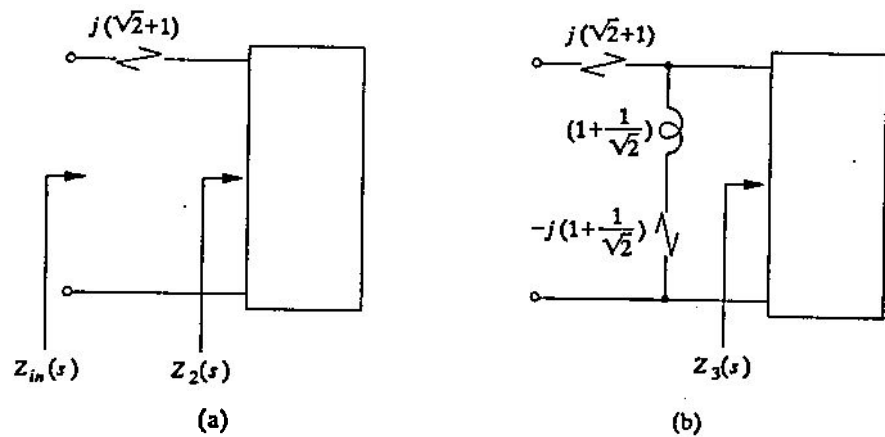
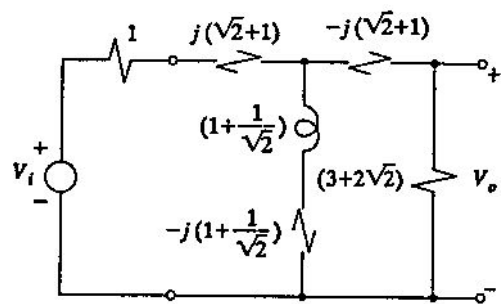


Fig. 2)



(c)

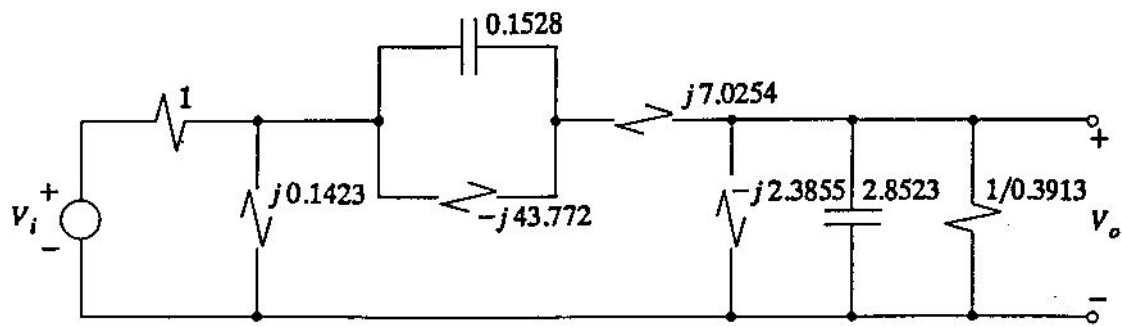


Fig. 22

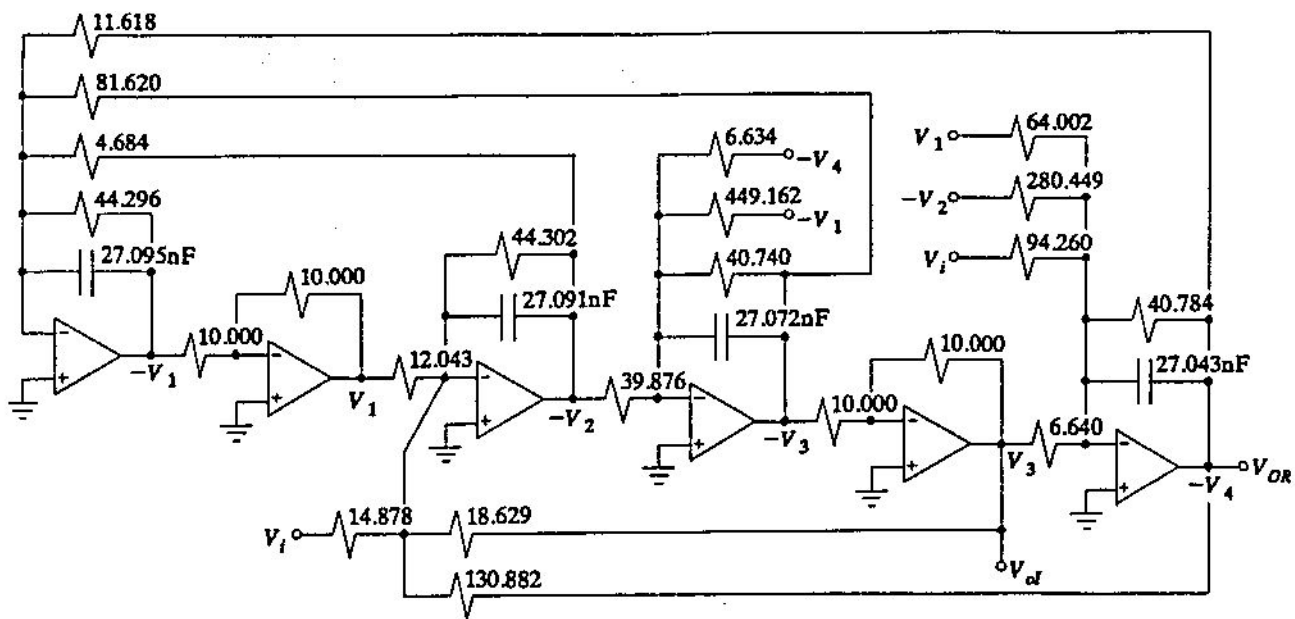


Fig. 23

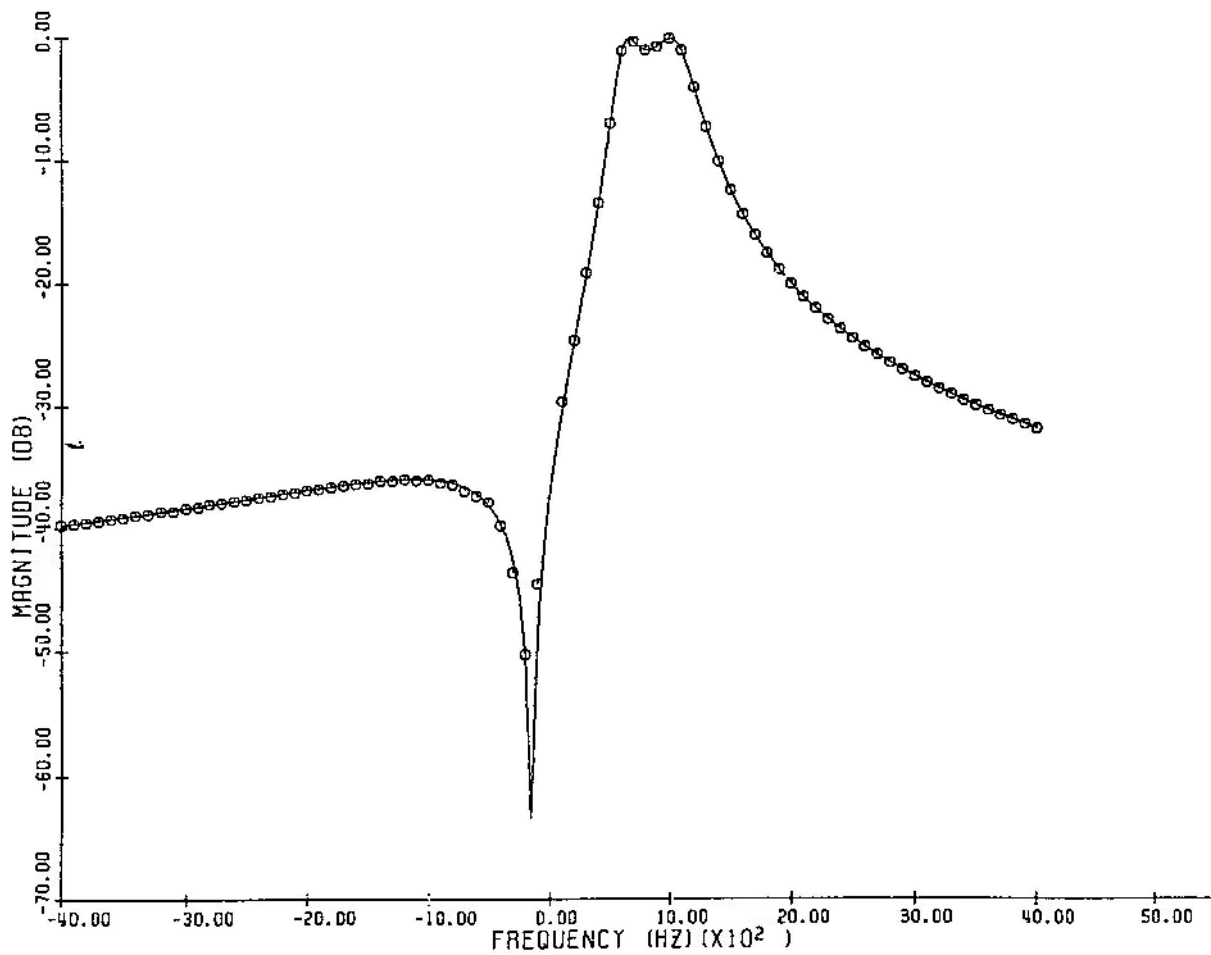


Fig. 24

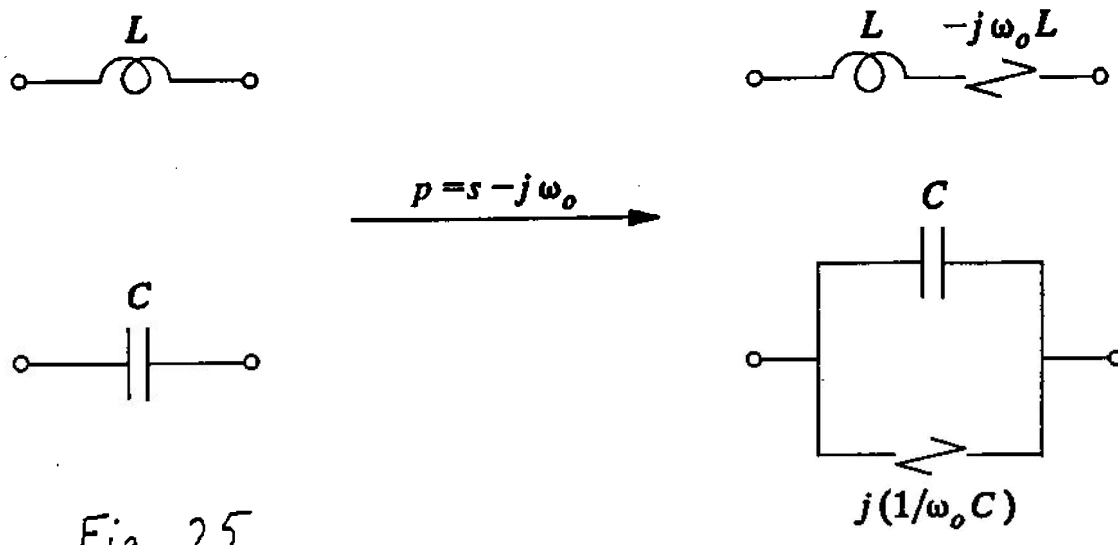


Fig. 25

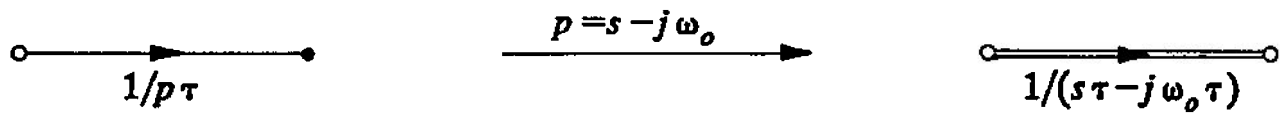


Fig. 26

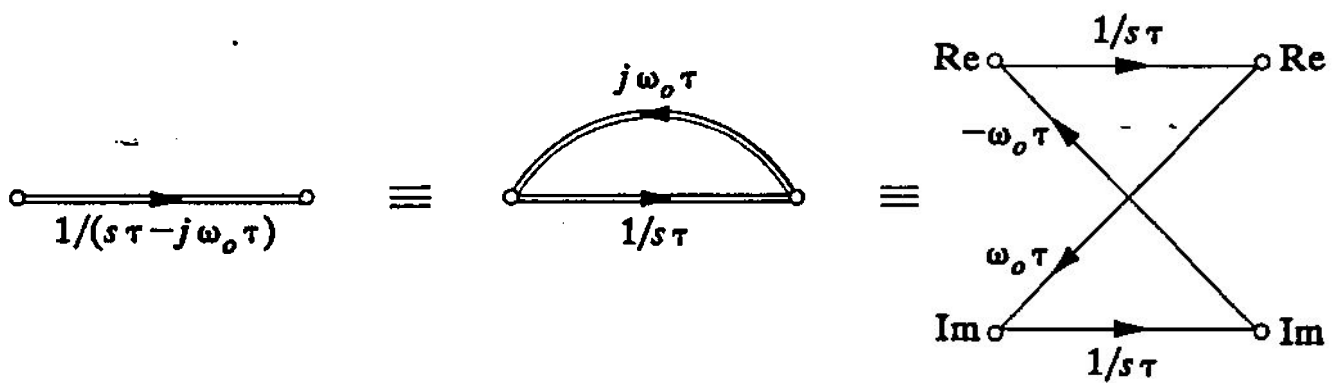


Fig. 27